



Calhoun: The NPS Institutional Archive

Theses and Dissertations

Thesis Collection

2012-09

Universal Zero Specular Reflection Curves for MetaMaterials

Ting, Choon Boon

Monterey, California. Naval Postgraduate School

<http://hdl.handle.net/10945/17469>



Calhoun is a project of the Dudley Knox Library at NPS, furthering the precepts and goals of open government and government transparency. All information contained herein has been approved for release by the NPS Public Affairs Officer.

Dudley Knox Library / Naval Postgraduate School
411 Dyer Road / 1 University Circle
Monterey, California USA 93943

<http://www.nps.edu/library>



NAVAL POSTGRADUATE SCHOOL

MONTEREY, CALIFORNIA

THESIS

UNIVERSAL ZERO SPECULAR REFLECTION CURVES FOR METAMATERIALS

by

Choon Boon Ting

September 2012

Thesis Advisor:
Second Reader:

David C. Jenn
Roberto Cristi

Approved for public release; distribution is unlimited

THIS PAGE INTENTIONALLY LEFT BLANK

REPORT DOCUMENTATION PAGE			<i>Form Approved OMB No. 0704-0188</i>	
Public reporting burden for this collection of information is estimated to average 1 hour per response, including the time for reviewing instruction, searching existing data sources, gathering and maintaining the data needed, and completing and reviewing the collection of information. Send comments regarding this burden estimate or any other aspect of this collection of information, including suggestions for reducing this burden, to Washington headquarters Services, Directorate for Information Operations and Reports, 1215 Jefferson Davis Highway, Suite 1204, Arlington, VA 22202-4302, and to the Office of Management and Budget, Paperwork Reduction Project (0704-0188) Washington DC 20503.				
1. AGENCY USE ONLY (Leave blank)		2. REPORT DATE September 2012	3. REPORT TYPE AND DATES COVERED Master's Thesis	
4. TITLE AND SUBTITLE Universal Zero Specular Reflection Curves for MetaMaterials			5. FUNDING NUMBERS	
6. AUTHOR(S) Choon Boon Ting				
7. PERFORMING ORGANIZATION NAME(S) AND ADDRESS(ES) Naval Postgraduate School Monterey, CA 93943-5000			8. PERFORMING ORGANIZATION REPORT NUMBER	
9. SPONSORING /MONITORING AGENCY NAME(S) AND ADDRESS(ES) N/A			10. SPONSORING/MONITORING AGENCY REPORT NUMBER	
11. SUPPLEMENTARY NOTES The views expressed in this thesis are those of the author and do not reflect the official policy or position of the Department of Defense or the U.S. Government.				
12a. DISTRIBUTION / AVAILABILITY STATEMENT Approved for public release, distribution is unlimited			12b. DISTRIBUTION CODE A	
13. ABSTRACT (maximum 200 words) Materials are generally classified in terms of their constitutive parameters, the complex permittivity ϵ and permeability μ , in the frequency domain. These parameters are used to determine the response of materials to electromagnetic (EM) radiation. Materials found in nature have positive real parts for both ϵ and μ . In recent years, researchers have shown that a new class of materials called metamaterials (MTMs), characterized by inclusions of various shapes and materials that are small compared to wavelength, result in an effectively homogeneous medium with the unique properties of negative real ϵ and μ which cause EM waves traveling through the medium to exhibit unusual characteristics. Zero specular reflection layers for four material types such as double positive (DPS), double negative (DNG), epsilon-negative (ENG) and mu-negative (MNG) materials are examined in this thesis. For each defined type of MTM, the transcendental equations are derived and solved numerically to generate curves for zero specular reflection. A MATLAB program was developed to generate universal curves for DPS, DNG, ENG, and MNG materials. The results were discussed and evaluated to determine wave behavior in each type of MTM as well as how they can be used as a matched-surface radar-absorbing material (RAM) for military application. The results were compared to published data.				
14. SUBJECT TERMS MetaMaterials, Negative Index, Universal Design Chart, Transcendental Equation, Complex Permittivity and Permeability, Constitutive Parameters			15. NUMBER OF PAGES 84	
			16. PRICE CODE	
17. SECURITY CLASSIFICATION OF REPORT Unclassified	18. SECURITY CLASSIFICATION OF THIS PAGE Unclassified	19. SECURITY CLASSIFICATION OF ABSTRACT Unclassified	20. LIMITATION OF ABSTRACT UU	

THIS PAGE INTENTIONALLY LEFT BLANK

Approved for public release; distribution is unlimited

**UNIVERSAL ZERO SPECULAR REFLECTION CURVES FOR
METAMATERIALS**

Choon Boon Ting
Civilian, Singapore Technologies Marine Ltd
B.E. (Electronic Engineering), University of Hull, UK, 2007

Submitted in partial fulfillment of the
requirements for the degree of

MASTER OF SCIENCE IN ELECTRICAL ENGINEERING

from the

**NAVAL POSTGRADUATE SCHOOL
September 2012**

Author: Choon Boon Ting

Approved by: Professor David C. Jenn
Thesis Advisor

Professor Roberto Cristi
Second Reader

Professor R. Clark Robertson
Chair, Department of Electrical and Computer Engineering

THIS PAGE INTENTIONALLY LEFT BLANK

ABSTRACT

Materials are generally classified in terms of their constitutive parameters, the complex permittivity ε and permeability μ , in the frequency domain. These parameters are used to determine the response of materials to electromagnetic (EM) radiation. Materials found in nature have positive real parts for both ε and μ . In recent years, researchers have shown that a new class of materials called metamaterials (MTMs), characterized by inclusions of various shapes and materials that are small compared to wavelength, result in an effectively homogeneous medium with the unique properties of negative real ε and μ which cause EM waves traveling through the medium to exhibit unusual characteristics.

Zero specular reflection layers for four material types such as double positive (DPS), double negative (DNG), epsilon-negative (ENG) and mu-negative (MNG) materials are examined in this thesis. For each defined type of MTM, the transcendental equations are derived and solved numerically to generate curves for zero specular reflection. A MATLAB program was developed to generate universal curves for DPS, DNG, ENG, and MNG materials. The results were discussed and evaluated to determine wave behavior in each type of MTM as well as how they can be used as a matched-surface radar-absorbing material (RAM) for military application. The results were compared to published data.

THIS PAGE INTENTIONALLY LEFT BLANK

TABLE OF CONTENTS

I.	INTRODUCTION.....	1
A.	BACKGROUND	1
B.	PREVIOUS WORK.....	4
C.	THESIS OBJECTIVE	5
D.	ORGANIZATION OF THESIS	5
II.	METAMATERIAL.....	7
A.	INTRODUCTION.....	7
B.	PERMITTIVITY AND PERMEABILITY	8
C.	CLASSIFICATION OF MATERIALS	10
D.	SUMMARY	14
III.	DESIGN FOR ZERO SPECULAR REFLECTION	15
A.	INTRODUCTION.....	15
B.	EQUATIONS FOR ZERO SPECULAR REFLECTION.....	17
C.	MATCHING LAYERS FOR PEC BACKING	19
D.	SUMMARY	22
IV.	SOLUTION RESULTS AND ANALYSIS	23
A.	SOLUTION APPROACH.....	23
B.	MATCHING LAYERS FOR DPS MATERIAL	25
C.	MATCHING LAYERS FOR DNG MATERIAL	29
D.	MATCHING LAYERS FOR ENG MATERIAL	33
E.	MATCHING LAYERS FOR MNG MATERIAL	35
F.	NUMERICAL SOLUTION FOR ENG AND MNG.....	36
G.	DISCUSSION OF SOLUTION METHODS.....	37
H.	SUMMARY	42
V.	CONCLUSION	43
A.	SUMMARY AND CONCLUSION	43
B.	FUTURE WORK.....	44
	APPENDIX.....	45
A.	MATLAB CODE FOR UNIVERSAL DESIGN CHART USING FSOLVE FUNCTION	45
B.	MATLAB CODE FOR DPS PERFECT ELECTRIC CONDUCTOR.....	52
C.	MATLAB CODE FOR DNG PERFECT ELECTRIC CONDUCTOR ...	52
D.	MATLAB CODE FOR MNG (SNG) PERFECT ELECTRIC CONDUCTOR	53
E.	MATLAB CODE FOR ENG (SNG) PERFECT ELECTRIC CONDUCTOR	53
F.	MATLAB CODE FOR CHECKING SOLUTION POINTS.....	53
G.	MATLAB CODE TO CHECK ON DPS LOOPS.....	54
H.	MATLAB CODE FOR UNIVERSAL DESIGN CHART USING SOLVE FUNCTION.....	57

LIST OF REFERENCES	59
INITIAL DISTRIBUTION LIST	61

LIST OF FIGURES

Figure 1.	An illustration of how waves attenuate when RAM is applied (After [1]).	1
Figure 2.	A negative-index MTM constructed using SRRs and wires embedded in fiberglass (From [3]).	3
Figure 3.	Refraction of an EM wave incident on a boundary between air and a DPS medium (top) and a DNG medium (bottom) (After [9]).	8
Figure 4.	Material diagram in ϵ - μ space for lossless MTMs (After [6]).	11
Figure 5.	Material diagram in A - B space for lossy MTMs (From [6]).	12
Figure 6.	(a) Specular-reflection layer with perfect electric conductor (PEC) backing and (b) equivalent transmission-line circuit (After [12]).	15
Figure 7.	Universal design chart for zero specular reflection with DPS material (From [2]).	16
Figure 8.	Sample plots generated from the MATLAB program for a DPS medium.	25
Figure 9.	MATLAB generated result on DPS material with $\tan \delta_{\epsilon} = 0.5$.	26
Figure 10.	DPS combined universal curves.	26
Figure 11.	Plots of the variables z and v in the complex plane.	27
Figure 12.	MATLAB generated result for DNG material with $\tan \delta_{\epsilon} = 0.5$.	29
Figure 13.	DNG combined universal curves.	30
Figure 14.	<i>fsolve</i> solutions for a DPS material with $\tan \delta_{\epsilon} = 0.01$, search start points of $x=10^{-4}$ and $y=10^1$.	38
Figure 15.	<i>fsolve</i> solutions for a DPS material with $\tan \delta_{\epsilon} = 0.01$, search start points of $x=10^{-0.35}$ and $y=10^{0.95}$.	39
Figure 16.	A curve generated for DPS material by solving the equation three times each with different initial start points.	40
Figure 17.	Curves generated using the <i>solve</i> function; $\tan \delta_{\epsilon} = 0.5$ (left) and $\tan \delta_{\epsilon} = 0.8$ (right).	41
Figure 18.	Simulation result generated using <i>fsolve</i> (left) and <i>solve</i> (right) function.	41

THIS PAGE INTENTIONALLY LEFT BLANK

LIST OF TABLES

Table 1.	Summary for lossless materials and handedness.	9
Table 2.	Summary of different type of MTM including lossy MTM.	12
Table 3.	Parameters for the modified MATLAB program for variable initial points.....	39
Table 4.	Color code for the results in Figure 16.	40

THIS PAGE INTENTIONALLY LEFT BLANK

LIST OF ACRONYMS AND ABBREVIATIONS

EM	Electromagnetic
RCS	Radar Cross Section
RAM	Radar Absorbing Material
MTM	Metamaterial
DNG	Double Negative
DPS	Double Positive
ENG	Epsilon-Negative
MNG	Mu-Negative
NIM	Negative-Index Materials
LH	Left-Handed
RH	Right-Handed
SRR	Split-Ring Resonator
PEC	Perfect Electric Conductor
MWS	Microwave Studio

THIS PAGE INTENTIONALLY LEFT BLANK

EXECUTIVE SUMMARY

In recent years, a new class of materials called metamaterials (MTMs) has been of increasing interest in research and development. The concept of such materials is to add inclusions of various shapes and composition that are small compared to wavelength, resulting in an effectively homogeneous medium with a desired relative permittivity $\epsilon_r = \epsilon'_r - j\epsilon''_r$ and permeability $\mu_r = \mu'_r - j\mu''_r$. MTMs are artificial media and their design can achieve unique properties of either positive or negative permittivity ϵ'_r or permeability μ'_r . With these unusual characteristics and properties, MTMs may achieve an effectively homogeneous uniform layer over a conductor to provide zero specular reflection over a wide range of frequencies. MTM has the potential for radar cross section (RCS) reduction, and its advantages over radar-absorbing material (RAM) include broader frequency ranges and aspect angles. In this thesis, we examine the characteristics of lossy MTMs and discuss how such material can be used as a RAM.

MTM characteristics and properties are analyzed and discussed in relation to plane-wave propagation. Natural materials such as double positive (DPS) materials that have $\epsilon'_r, \mu'_r > 0$ are referred to right-hand (RH) materials since the electric field vector, magnetic field vector, and the direction of power flow given by the Poynting vector ϵ_r is according to the RH rule. Double negative (DNG) materials that have $\epsilon'_r, \mu'_r < 0$ are referred to as left-handed (LH) materials since the propagation vector ~~is~~ is in the opposite direction to ϵ_r . Single negative (SNG) materials can be of either type, and some materials change from LH to RH and back again as the frequency changes. The four types of MTM materials (DPS, DNG, epsilon-negative (ENG), and mu-negative (MNG)), of different permeability and permittivity combinations are demonstrated to be either LH or RH. One effect on a propagating wave is the reversal of Snell's law at an interface between DPS and DNG materials.

A new material diagram, referred to as A - B phase space, was introduced for classifying lossy MTMs and was used in this research. The parameters A and B are

defined by $A = \mu'_r \varepsilon'_r - \mu''_r \varepsilon''_r$ and $B = \mu''_r \varepsilon'_r + \mu'_r \varepsilon''_r$. The sign of B defines the material handedness, RH or LH. The material is RH when $B > 0$ and LH when $B < 0$. However, the sign of A can be either positive or negative for both DPS and DNG but has to be negative for both ENG and MNG.

The design for zero specular reflection using a homogeneous uniform dielectric/magnetic absorber is analysed and presented in accordance with transmission line theory, and universal design charts for zero specular reflection layers that reduce the normal incidence specular reflection to zero were generated. The transcendental equation was derived for the four types of MTM matching layers to produce zero specular reflection of a layer with conductor backing. Each solution gives a proper combination of the six design parameters involved: wavelength λ , layer thickness t , real and imaginary components of the complex dielectric constant, and the magnetic permeability ($\varepsilon'_r, \varepsilon''_r, \mu'_r$, and μ''_r) for zero reflection [2].

The six design parameters were reduced to four by rescaling with the factor t/λ to get new parameters: $a = (t/\lambda) \varepsilon'_r$, $b = (t/\lambda) \varepsilon''_r$, $x = (t/\lambda) \mu'_r$, and $y = (t/\lambda) \mu''_r$. The transcendental equations of the form $j\sqrt{(x-jy)/(a-jb)} \tan\left(2\pi\sqrt{(x-jy)(a-jb)}\right) = 1$ were solved numerically using the MATLAB *fsolve* and *solve* functions in order to generate universal curves. Curves are plotted in the $x-y$ plane for various values of a and b as shown in Figure 1 for a DPS material.

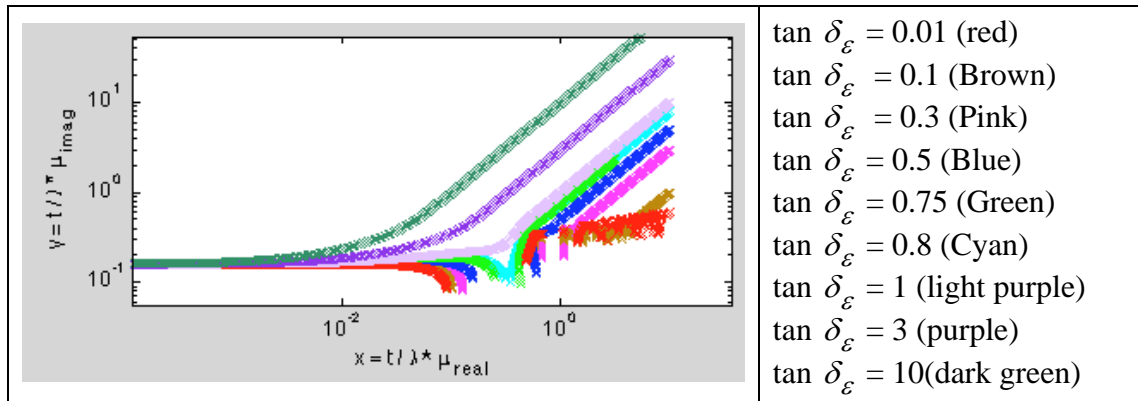


Figure 1 : DPS combined universal curves ($\tan \delta_\varepsilon = b/a$).

The DPS curves show similar results as compared to published data [2] except for small values of y . This is attributed to non-convergence of the numerical solution algorithms. The results verify that the DNG equation is the complex conjugate of the DPS equation. Therefore, one set of curves can be used for both DPS and DNG cases if the proper substitution of signs is made for a, b, x and y . The numerical algorithm indicated that there are no physical solutions to the ENG and MNG equations. It should be possible to verify this result by mathematical proof.

THIS PAGE INTENTIONALLY LEFT BLANK

ACKNOWLEDGMENTS

I would like to express my sincere gratitude to Professor David C. Jenn, for his patience and guidance in this thesis. His valuable knowledge in metamaterials, electromagnetic and MATLAB gave me the confidence and motivation to complete this thesis. Professor Jenn has a sense of devotion, patience, and willingness to share information that is indeed remarkable. Without Professor Jenn's advice and assistance, this thesis would not have been completed.

I would like to thank Professor Roberto Cristi for being my second reader. I appreciated his sharing of knowledge and explanations of the mathematical, theoretical background of this thesis.

I would like to thank my lovely wife, Tina Ong, for her support and understanding throughout my thesis research. She took care of family needs and did well in educating our lovely baby daughter, Wen Fang. Her constant and unconditional support gave me great motivation to complete the thesis, especially when my grandma passed away and mother had a stroke. I also thank my parents, Tony Ting and Li Chin, who always taught me the real values and meaning of life.

Finally, I would like to thank my boss, Mr. Tan Ching Eng, and superior, Mr. Steve Wong, from Singapore Technologies Marine Ltd, for providing me the opportunity to earn a double master's degree from the National University of Singapore and Naval Postgraduate School.

THIS PAGE INTENTIONALLY LEFT BLANK

I. INTRODUCTION

A. BACKGROUND

In modern warfare, the military has been confronted with an increasingly complex electromagnetic (EM) environment. An important aspect of this is the platform (e.g., ship) radar signature or radar cross section (RCS). With advances in radar technology, the RCS of a target is a critical consideration—it is necessary to reduce RCS to increase survivability. With reduction in a ship's signature, there is less chance of being detected by hostile radar and engaged by missiles.

There are various ways to reduce the ship's signature. Mainly this is achieved by shaping (e.g., adapt a certain slope angle on the ship hull and deckhouse design during construction) or by applying radar-absorbing material (RAM) to the scattering area onboard the ship. RAM absorbs radar energy and is used to reduce the echo returns to a hostile radar, as shown in Figure 1. In this figure, (U^-, p^-) represent, respectively, the incident, reflected, and transmitted electric-field components.

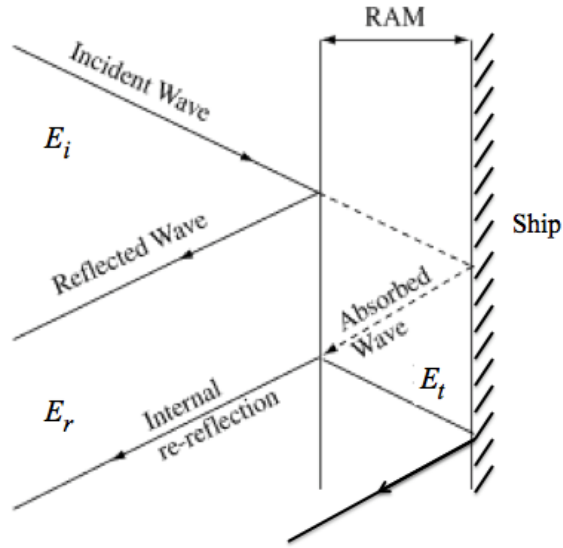


Figure 1. An illustration of how waves attenuate when RAM is applied (After [1]).

Applied to a platform, this technology makes hostile radar less likely to detect a stealth ship, as the radar echo received from the targeted platform has been reduced.

Conventional RAM can be thick and heavy when used in the amount needed for adequate RCS reduction. Recently, newly engineered materials have shown promise in RCS reduction in the form of thin layers. According to [2], “It is theoretically possible to design a homogeneous uniform dielectric/magnetic electromagnetic wave absorber layer that will reduce the normal-incidence specular reflection from a perfectly reflective substrate to zero at a specified frequency (or wavelength).”

For the purpose of classifying the EM behavior of materials, the complex constitutive parameters of permittivity \vec{D} and permeability \vec{B} are specified as

$$\left(\vec{D} = \epsilon \vec{E}, \quad \vec{B} = \mu \vec{H} \right) \quad (1)$$

and

$$\epsilon_0 = 8.854 \times 10^{-12} \text{ F/m} \quad (2)$$

where $\epsilon_0 = 8.854 \times 10^{-12} \text{ F/m}$ and $\mu_0 = 4\pi \times 10^{-7} \text{ H/m}$ are free-space permittivity and permeability, respectively. The negative imaginary part is due to the chosen time convention $e^{-j\omega t}$. The new class of material is called metamaterial (MTM). The concept for such materials is to add inclusions of various shapes and composition that are small compared to a wavelength, resulting in an effectively homogeneous medium with the desired relative permittivity ϵ_r and permeability μ_r . The inclusions change the electric and magnetic susceptibilities of the medium. MTM has the potential for RCS reduction and advantages over RAM that include broader frequency ranges and aspect angles.

MTMs are artificial media that can be designed to achieve the unique properties of negative real parts of permittivity ϵ'_r and permeability μ'_r . Negative permittivity and permeability are not normally found in nature. Negative values can be achieved by using copper split-ring resonators (SRRs) and wires embedded in a fiberglass circuit board, as shown in Figure 2. Copper wires provide negative electric permittivity, while the SRR provides the increased magnetic response and negative permeability of the MTM. The MTM in Figure 2 consists of three planar concentric rings per unit cell facing in opposite directions (i.e., a thickness of three cells). The unit cell dimensions are usually much

smaller than the operating wavelength. The challenge is to fabricate MTMs for increasingly smaller wavelengths and wider bandwidth capabilities.

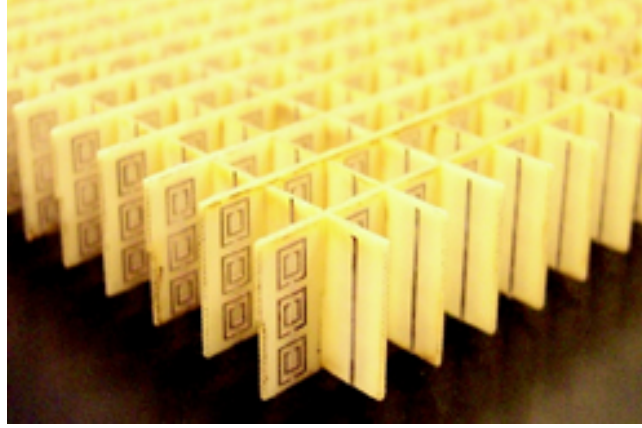


Figure 2. A negative-index MTM constructed using SRRs and wires embedded in fiberglass (From [3]).

MTMs can be designed to have either $\epsilon'_r < 1$ or $\mu'_r < 1$ (single negative (SNG)), or both $\epsilon'_r < 1, \mu'_r < 1$ (double negative (DNG)). The most popular class of MTMs studied in recent years is DNG. In comparison to the positive permittivity and permeability achieved from double positive (DPS) materials, i.e., normal right-handed (RH) materials, the negative permittivity and permeability of DNG material causes the electromagnetic wave phase fronts to travel in the opposite direction to the power flow due to the negative index of refraction. For a lossless DNG material ($\epsilon'_r < 0, \mu'_r < 0$), the index of refraction is

$$n = \sqrt{(-\epsilon'_r)(-\mu'_r)} = \sqrt{(-1)^2 |\epsilon'_r| |\mu'_r|} = -\sqrt{|\epsilon'_r| |\mu'_r|}. \quad (3)$$

DNG materials are also known as negative-index materials (NIM), or left-handed (LH) materials. With such unusual characteristics and properties, MTMs can be designed and engineered to achieve an effectively homogeneous uniform dielectric electromagnetic layer which provides zero specular reflection over a wide range of frequencies. Such unique MTM properties can be used in many different applications, such as novel antenna shapes and sizes, shielding, perfect lenses, and resonators.

B. PREVIOUS WORK

This research is part of an ongoing project that started with a thesis by Feng [4] on extracting the material constitutive parameters from scattering parameters (S-parameters). Doumenis [5] continued with the properties and applications of lossy MTMs. Musal and Smith [2] used a zero-specular-reflection analysis to generate universal curves for lossy dielectric and magnetic layers based on six independent system parameters: layer thickness t , wavelength λ , ϵ_r . From [2], universal curves can be used to determine the type of material configuration and electromagnetic parameter values that can produce zero specular reflection. Further studies were conducted to use the universal design chart to analyze the EM wave scattering. “This graphic aid not only simplifies the design process, but also provides an overall view of the interrelated numerical values of material properties required to implement various specular electromagnetic absorber design concept.” [2]

Several methods to determine the effective permittivity and permeability of MTMs were examined in [4]. Further studies were conducted using CST Microwave Studio software to obtain the simulated S-parameters of normal and MTM materials in both free space and rectangular waveguide environments. An algorithm was developed to extract the effective ϵ_r and μ_r from the S-parameters.

Zero specular reflection layers using double negative materials were examined in [5]. The zero specular reflection equations were used to examine the symmetry between universal design charts for DPS and DNG materials. Further studies were conducted to determine the relationship of effective permittivity and permeability of normal materials to those of MTMs from measured or simulated scattering parameters.

Lee and Park [6] derived a general propagation constant for the four types of lossy materials, mainly DPS, DNG, epsilon-negative (ENG), and mu-negative (MNG). Their research also demonstrated how the propagation constant is affected by the material constants and the loss terms of ϵ and μ . A new graphical A–B space was introduced to distinguish lossy DPS, DNG, and SNG material types with their handedness, RH or LH.

According to Holloway [7], we find that metasurfaces (or metafilms) can be used in place of MTMs in many applications. Metafilm refers to thin metamaterial that is only one unit-cell thick. “Metasurfaces have the advantage of taking up less physical space than do full three-dimensional MTM structures.” [7] Further studies were conducted on metasurface characterization, various applications, and how metasurfaces are distinguished from conventional frequency-selective surfaces. The appeal of metafilms for RCS treatments is their thin, lightweight profile when applied to surfaces.

C. THESIS OBJECTIVE

The objective of this thesis is to investigate MTM RAM designs for low RCS applications. Sets of universal design curves for zero specular reflection MTMs, such as double negative and single negative are generated by solving a transcendental equation. Using each defined type of MTM, we derived and numerically solved the transcendental equations to generate curves for zero specular reflection. Each solution gives a proper combination of the six design parameters involved: wavelength, layer thickness, real and imaginary components of the complex dielectric constant, and the permeability for zero reflection [2]. The multiple results of individual types of MTM are merged to form a universal design chart. The results are discussed and evaluated to determine each type of MTM characteristic and how they can be used as a matched-surface RAM for military applications.

D. ORGANIZATION OF THESIS

In Chapter I, the application of RAM in modern warfare is introduced, along with how MTMs might be used to achieve zero specular reflection. The research objective and outline are also highlighted in this chapter.

In Chapter II, the background theory of wave behavior in the various MTMs is described, with a discussion of the interaction of waves with various MTMs, the impact of positive and negative permittivity and permeability, and the classifications of MTM behavior.

An analysis of RAM, based on matched-wave impedance and zero specular reflection conditions, is contained in Chapter III. There is a discussion of the advantages and disadvantages of the two approaches. Zero specular reflection numerical equations are derived and used for each MTM to determine a combination of parameters for absorption, based on solving a transcendental equation.

Numerical solution results and analysis of the matching layers for the four types of MTMs is contained in Chapter IV. There are four plots for each set of solutions that characterize the material and wave propagation. The multiple results from individual solutions are merged to form a universal design chart for zero reflection.

This research is summarized in Chapter V, with conclusions and recommendations for future research.

II. METAMATERIAL

In this chapter, background theory on the classification of MTMs and how waves propagate in the four types of MTMs are discussed. This discussion forms a foundation for better understanding of the mathematical equations employed, which relate to the universal curves in later chapters.

A. INTRODUCTION

The history of MTM dates back to 1967, when a Russian physicist named Victor Georgievich Veselago [8] showed that materials, apart from the usual case of positive permittivity ϵ and permeability μ , can also be negative for both quantities, yielding a negative refractive index. Veselago demonstrated the behavior of wave propagation in two substances of different ϵ and μ as being RH or LH. The experiment concluded that, in a LH substance, the phase velocity \vec{U}_p is opposite the energy flux given by the Poynting vector \vec{E} . Veselago named the new material “negative-index materials” or “left-handed materials,” since the vector triplet, electric field vector \vec{E} , magnetic field vector \vec{H} , and power flow \vec{k} formed a LH set.

Veselago also experimented with the refraction of a ray at a boundary between two media of different handedness. The experiment demonstrated that waves impinging on the boundary between a normal material and negative refractive index material are refracted in the reverse direction at the interface of the two materials. This is indicated at the bottom of Figure 3.

Veselago’s analysis of the double-negative ϵ and μ was considered nothing more than an interesting idea for more than thirty years. In 1999, J. B. Pendry managed to show how materials could be created artificially with double-negative properties [9] [10]. In 2000, Pendry showed how negative refraction makes a perfect lens and proposed to use MTMs to make such a lens [9]. In the same year, D. R. Smith and a team of researchers demonstrated a composite medium that exhibited negative values of effective

ε and μ [11]. The success of their microwave experiment stimulated further research into new MTMs.

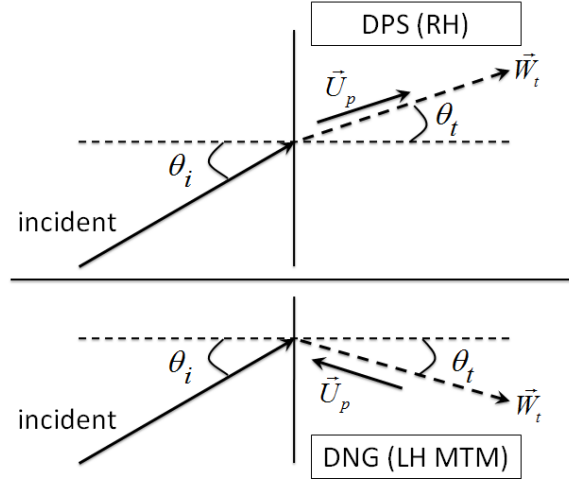


Figure 3. Refraction of an EM wave incident on a boundary between air and a DPS medium (top) and a DNG medium (bottom) (After [9]).

B. PERMITTIVITY AND PERMEABILITY

Any type of material can generally be classified in terms of its constitutive parameters ε and μ . Classification of materials includes linear or nonlinear, homogeneous or inhomogeneous, and isotropic or anisotropic, to name a few. The Tellegen representation is able to cover all cases represented in the form of a matrix, with the electric and magnetic fields \mathcal{V} related to electric and magnetic flux densities

$\mathcal{E} = \begin{pmatrix} \varepsilon_{xx} & \varepsilon_{xy} & \varepsilon_{xz} \\ \varepsilon_{yx} & \varepsilon_{yy} & \varepsilon_{yz} \\ \varepsilon_{zx} & \varepsilon_{zy} & \varepsilon_{zz} \end{pmatrix}$ by

$$\mu_r = \begin{pmatrix} \mu_{xx} & \mu_{xy} & \mu_{xz} \\ \mu_{yx} & \mu_{yy} & \mu_{yz} \\ \mu_{zx} & \mu_{zy} & \mu_{zz} \end{pmatrix}. \quad (4)$$

where the off-diagonal blocks are zero for the MTMs considered.

For example, the Cartesian system vectors and matrices in Eq. (4) have the forms

$$\boldsymbol{\varepsilon}_{ij}, \boldsymbol{\varepsilon}_r = \begin{pmatrix} \varepsilon_{xx} & \varepsilon_{xy} & \varepsilon_{xz} \\ \varepsilon_{yx} & \varepsilon_{yy} & \varepsilon_{yz} \\ \varepsilon_{zx} & \varepsilon_{zy} & \varepsilon_{zz} \end{pmatrix} \text{ and } \boldsymbol{\mu}_r = \begin{pmatrix} \mu_{xx} & \mu_{xy} & \mu_{xz} \\ \mu_{yx} & \mu_{yy} & \mu_{yz} \\ \mu_{zx} & \mu_{zy} & \mu_{zz} \end{pmatrix}. \quad (5)$$

The elements found in the matrix $\boldsymbol{\varepsilon}_{ij}$ and $\boldsymbol{\mu}_{ij}$, where i and $j = x, y$, or z , are the complex relative values. For lossless media, the imaginary terms are zero. For DPS materials, the real parts are positive. Conversely, for DNG materials, both real parts are negative. Finally, for a SNG material, one of the real parts is positive and one negative. These cases are summarized in Table 1. Note that in a lossy passive material, the imaginary terms are negative for all material types. Often, loss tangents are used to describe material losses. The dielectric loss tangent is

$$A-B \quad (6)$$

and the magnetic loss tangent is

$$\tan \delta_\mu = \frac{\mu_r''}{\mu_r'}. \quad (7)$$

Table 1. Summary for lossless materials and handedness.

Type of material		Real Part of Permittivity ε and permeability μ	Plane-wave propagation
DPS		$\varepsilon'_r > 0, \mu'_r > 0$	RH
DNG		$\varepsilon'_r < 0, \mu'_r < 0$	LH
SNG	ENG	$\varepsilon'_r < 0, \mu'_r > 0$	Evanescent
	MNG	$\varepsilon'_r > 0, \mu'_r < 0$	Evanescent

Natural materials such as DPS materials are referred to as RH materials due to the vectors of the electric field, magnetic field, and power flow (given by Poynting vector β) for a plane wave traveling in the positive z direction follow the RH rule. The Poynting vector is given by

$$\omega = 2\pi f. \quad (8)$$

The propagation vector k is in the same direction as β and given by

$$\vec{k} = \hat{k} k_o \sqrt{\epsilon'_r \mu'_r} \quad (9)$$

where $k_o = \omega \sqrt{\mu_o \epsilon_o}$, $\omega = 2\pi f$, and λ_o = free space wavelength.

DNG materials are referred to LH materials since the propagation vector k is in the opposite direction of β , forming a LH system with β and k :

$$\vec{k} = \hat{k} k_o \sqrt{|\epsilon'_r| |\mu'_r|} = -\hat{k} k_o n. \quad (10)$$

ENG materials can be of either type, and some materials change from LH to RH and back again as frequency changes.

C. CLASSIFICATION OF MATERIALS

The electromagnetic properties of a material are determined by its ϵ and μ . The material diagram in ϵ - μ space for lossless MTMs can be classified into four types depending on the signs of ϵ and μ as shown in Figure 4 [6]. However, the resonant structures of MTM properties are always dispersive and lossy. Therefore, the classification of Figure 4 is not valid for lossy MTMs.

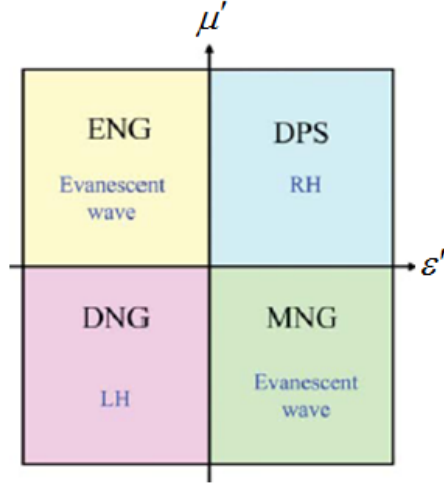


Figure 4. Material diagram in ε - μ space for lossless MTMs (After [6]).

The general propagation constant γ for all four types of lossy MTMs (DPS, DNG, ENG, and MNG) was derived by Lee and Park [6]. After an investigation of how the propagation constant is affected by material constants and by the loss terms of ε and μ , a new phase space for classifying lossy MTMs was introduced and is used in this research.

The propagation constant γ for a material can be written explicitly as

$$\alpha \quad (11)$$

where α is the attenuation constant (Np/m), and β is the phase constant (rad/m). Furthermore, we can write

$$\gamma = \pm j\omega\sqrt{\varepsilon_r\varepsilon_o\mu_r\mu_o} = \pm jk_o\sqrt{(\varepsilon'_r - j\varepsilon''_r)(\mu'_r - j\mu''_r)} = \pm jk_o\sqrt{A - jB} \quad (12)$$

where

$$A = \mu'_r\varepsilon'_r - \mu''_r\varepsilon''_r \quad (13)$$

and

$$B = \mu''_r\varepsilon'_r + \mu'_r\varepsilon''_r. \quad (14)$$

The square root can either be positive or negative, so there is a \pm sign added in Eqs. (11) – (12). The solution that gives a positive attenuation is a real solution, due to conservation of energy. Therefore, the correct sign of γ is paired with positive α .

Writing γ in rectangular form, we can examine the special cases for attenuation α and phase constant β . They are summarized in Table 2. In Figure 5, the material types are shown in A - B space, where A and B are defined in Eqs. (13) – (14).

Table 2. Summary of different type of MTM including lossy MTM.

Type of MTM		ϵ - μ Space	Attenuation and Phase constant	A - B Space
DPS		$\epsilon'_r \mu'_r > 0$	$\alpha > 0$ and $\beta > 0$	RH
DNG		$\epsilon'_r \mu'_r < 0$	$\alpha > 0$ and $\beta < 0$	LH
SNG	ENG	Electric losses: $\alpha \geq 0$	$\alpha > 0$ and $\beta > 0$	RH
		magnetic losses: $e - \gamma z$	$\alpha > 0$ and $\beta < 0$	LH
	MNG	Electric losses: $e - \gamma z$	$\alpha > 0$ and $\beta < 0$	LH
		magnetic losses: $\alpha \geq 0$	$\alpha > 0$ and $\beta > 0$	RH

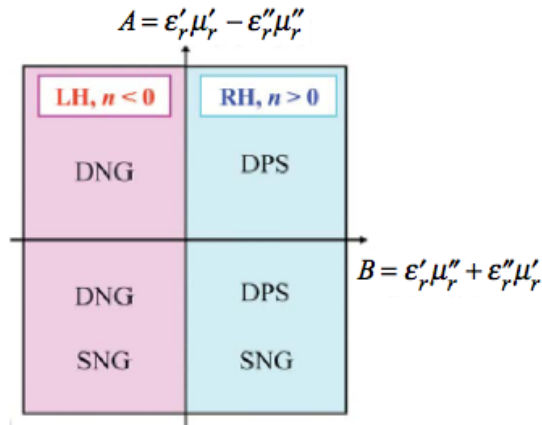


Figure 5. Material diagram in A - B space for lossy MTMs (From [6]).

For lossless DPS with the condition $\Gamma = \frac{Z_{in} - Z_o}{Z_{in} + Z_o} = 0$, $Z_d = \frac{Z_L + jZ_o \tan(\theta)}{Z_o + jZ_L \tan(\theta)}$ and Z_L and lossless DNG with condition Z_d , $Z_o = \frac{Z_L + jZ_o \tan(\theta)}{Z_o + jZ_L \tan(\theta)}$ and Z_L , the sign of $\Re\left\{\frac{\mu_z}{\epsilon_z}\right\}$ is used to determine the direction of wave propagation. It is important to note that DPS has positive $\Re\left\{\frac{\mu_z}{\epsilon_z}\right\}$, while DNG has negative $\Re\left\{\frac{\mu_z}{\epsilon_z}\right\}$.

For lossy DPS $\Gamma = \frac{Z_{in} - Z_o}{Z_{in} + Z_o} = 0$, $Z_o = \sqrt{\frac{\mu_o}{\epsilon_o}}$, and $\Re\left\{\frac{\mu_z}{\epsilon_z}\right\} > 0$, this material is defined as a RH material, while DNG has Z_d , $Z_o = \sqrt{\frac{\mu_o}{\epsilon_o}}$, and $\Re\left\{\frac{\mu_z}{\epsilon_z}\right\} < 0$, which is defined as a LH material because $\Re\left\{\frac{\mu_z}{\epsilon_z}\right\}$ is always negative.

For lossless ENG and MNG with Z_{in} / Z_o , Γ , and $\Gamma = \frac{Z_m / Z_o - 1}{Z_m / Z_o + 1}$, waves cannot propagate in these materials because $\Gamma = \frac{Z_m / Z_o - 1}{Z_m / Z_o + 1}$. These are evanescent waves that exhibit exponential decay with distance from the boundary where the wave was formed.

For lossy ENG, there are two types of losses: electrical and magnetic. For ENG with electrical losses under the condition Z_L , $\Re\left\{\frac{\mu_z}{\epsilon_z}\right\} > 0$ and λ , the waves propagate exponentially within the propagation region since $\Re\left\{\frac{\mu_z}{\epsilon_z}\right\} > 0$ and the sign for dielectric loss tangent is positive. Therefore, this material is defined as RH. For ENG with magnetic losses under the condition t , $\Re\left\{\frac{\mu_z}{\epsilon_z}\right\} < 0$ and $\frac{Z_d \tanh(\gamma t)}{Z_o} - 1 = 0$, the sign of $\Re\left\{\frac{\mu_z}{\epsilon_z}\right\}$ is negative ($\Re\left\{\frac{\mu_z}{\epsilon_z}\right\} < 0$), so this material is defined as LH and the sign of the dielectric loss tangent is negative. With both type of losses, it is important to note that ENG material can be either RH or LH material. ENG has the characteristic of large attenuation since Z_d is large.

Similar to lossy ENG, MNG has electric and magnetic losses. For MNG with magnetic losses with the condition $\sqrt{\frac{(\mu_r' - j\mu_r'')}{(\epsilon_r' - j\epsilon_r'')}} \tanh(jk_o t \sqrt{(\epsilon_r' - j\epsilon_r'')(\mu_r' - j\mu_r'')}) - 1 = 0$, $j \sqrt{\frac{(\mu_r' - j\mu_r'')}{(\epsilon_r' - j\epsilon_r'')}} \tan\left(\frac{2\pi}{\lambda_o} \sqrt{(\epsilon_r' - j\epsilon_r'')(\mu_r' - j\mu_r'')}\right) - 1 = 0$, this material is defined as RH. For MNG with electric losses with the condition $\tan \delta_\epsilon = \frac{b}{a}$, $j \sqrt{\frac{(x - jy)}{(a - jb)}} \tan(2\pi \sqrt{(x - jy)(a - jb)}) = 1$, the sign of $\Re\left\{\frac{\mu_z}{\epsilon_z}\right\}$ is negative ($\Re\left\{\frac{\mu_z}{\epsilon_z}\right\} < 0$), so this material is defined as LH.

D. SUMMARY

In this chapter, an introduction to MTM and their ε and μ properties was presented. The classification of lossy materials in terms of the signs of ε and μ and in terms of the A and B parameters was given. The general propagation constant equation for lossy MTMs (DPS, DNG, ENG, and MNG) and the material diagram in A - B space for lossy MTMs and their handedness were discussed. An important note is that the sign of $\frac{A}{B}$ defines the material handedness, RH or LH. The material is RH when $\frac{A}{B} > 0$ and LH when $\frac{A}{B} < 0$. However, the sign of $\frac{A}{B}$ can be either positive or negative for both DPS and DNG but must be negative for both ENG and MNG.

In the next chapter, the reflection from a RAM layer of MTM is addressed.

III. DESIGN FOR ZERO SPECULAR REFLECTION

In this chapter, the design for zero specular reflection using a homogeneous, uniform dielectric/magnetic-wave absorber is presented in accordance with transmission-line theory. The solutions to the equations are used to generate universal design charts for zero specular reflection layers that will reduce the normal incidence specular reflection. In addition, the equations for the DNG and SNG layers are programmed in MATLAB to generate individual curves on a universal chart.

A. INTRODUCTION

When EM waves impinge onto a RAM panel, there is some reflection and transmission at the outer face. The transmitted part is reflected at the back face. Therefore, the EM field within the absorber layer consists of the sum of forward and backward traveling waves, as shown previously in Figure 1 and presented in more detail in Figure 6.

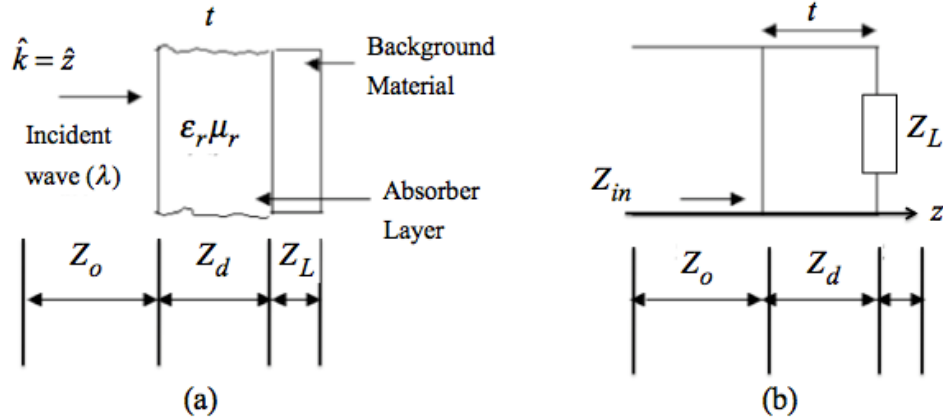


Figure 6. (a) Specular-reflection layer with perfect electric conductor (PEC) backing and (b) equivalent transmission-line circuit (After [12]).

The design parameters required to generate the universal curves are the six independent system parameters for the transmission-line model, shown in Figure 6. They are wavelength λ , layer thickness t , and the real and imaginary components of the

complex dielectric constant and magnetic permeability ($\epsilon'_r, \epsilon''_r, \mu'_r$, and μ''_r). The six parameters can be combined to yield four new parameters by normalizing ϵ and μ by $(\epsilon_0 \mu_0)$. The normalized parameters are

$$a, b, x, \text{ and } y \quad (15)$$

$$Z_L = 0 \quad (16)$$

$$Z_{in} - Z_o = 0 \quad (17)$$

$$a, x < 0 \quad (18)$$

The curves in Figure 7 comprise a universal chart, with z_L plotted on the horizontal axis and z_o on the vertical axis of a two-dimensional, Cartesian coordinate system. The relationship between the equations and the six design parameters form the basis of this research.

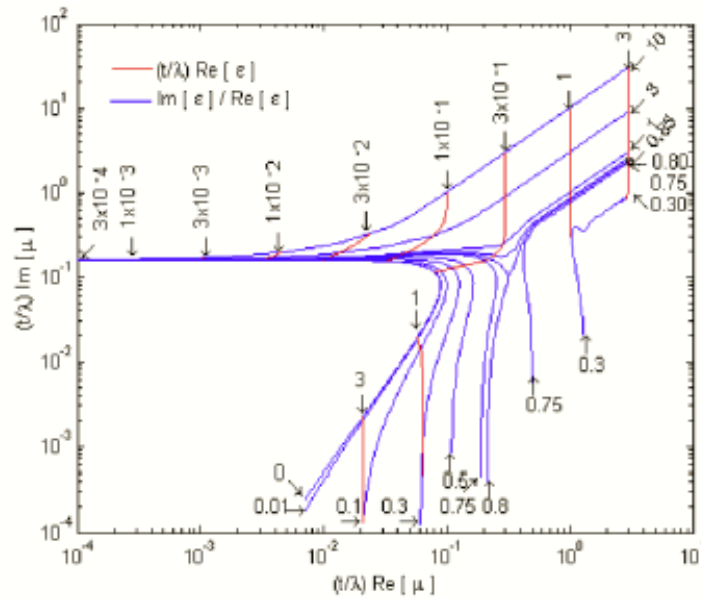


Figure 7. Universal design chart for zero specular reflection with DPS material (From [2]).

The individual curves generated for the universal design chart fall into three distinctly different parameter regions (first presented by Musal [2]). The left curve region represents thin absorbers, less than $1/4$ -wavelength thick. Therefore, the dielectric constant value is less than unity when the curve travels towards the extreme left. The topside curve region represents matched-characteristic impedance absorbers. The chart in Figure 7 shows curves for dielectric loss tangent values up to ten. A sequence of similar curves of higher-value dielectric loss tangents could fill the entire top region. The lower-right curve region represents resonant $1/4$ -wavelength absorbers.

B. EQUATIONS FOR ZERO SPECULAR REFLECTION

A typical RAM layer on a backing material of PEC is shown in Figure 6. According to [2], we see that there are two design considerations for effective EM absorber operations that will reduce specular reflection from highly reflective surfaces. Two different conceptual approaches to reduce specular reflection are matched-characteristic impedance and matched-wave impedance. The idea behind matched-characteristic impedance is to make the material and free-space intrinsic impedance equal to each other. Under the condition of equal impedance, both the material dielectric constant and magnetic permeability are also equal. Therefore, there is no front-surface reflection from the layer. To further reduce the incident wave to an acceptable low amplitude, the layer thickness must provide internal attenuation along the round-trip path. The second concept, matched-wave impedance, is to make the wave impedance equal for the front surface of a reflector-backed reflector layer and free space. With such an application of equal wave impedance, there is no reflection.

The imaginary parts ε_r'' and μ_r'' in Eq. (1) and Eq. (2) represent dielectric and magnetic losses. The propagation constant is given by Eq. (12). A passive medium must always have $\alpha \geq 0$, because the plane-wave propagation in the positive z -direction is of the form $e^{-\alpha z} e^{j(\omega t - \beta z)}$. Therefore, the sign of the square root in Eq. (12) must be chosen so

that $\alpha \geq 0$, and the same sign is applied to β . The sign of β determines whether the material behavior is RH or LH.

Using the transmission-line model in Figure 6, we have the reflection coefficient at the front face of the layer for normal incidence as

$$j\sqrt{\frac{Z}{v}} \tan(2\pi\sqrt{Zv}) = 1. \quad (19)$$

where

$$Z_{in} = Z_d \frac{Z_L + Z_d \tanh(\gamma t)}{Z_d + Z_L \tanh(\gamma t)}. \quad (20)$$

The backing material has impedance Z_o , and Z_d represents the impedance of the coating layer

$$Z_d = \sqrt{\frac{\mu_r}{\epsilon_r}} Z_o \quad (21)$$

where $Z_o = \sqrt{\frac{\mu_o}{\epsilon_o}}$. Therefore,

$$\tan \delta_\epsilon = \tan \delta_\mu. \quad (22)$$

According to [2], for the second concept (the matched-wave impedance method) we make wave impedance for the front surface of a reflector-backed layer and free space equal. With equal wave impedance, there is no reflection. The terms in the reflection coefficient Eq. (19) need to be normalized by Z_o so that there is no reflection for a given Z_L , when $Z_{in}/Z_o = 1$ and the reflection coefficient Γ is zero. The reflection coefficient equation after normalization by Z_o is

$$\tan \delta_\epsilon = 0. \quad (23)$$

Thus, the condition for no reflection for a given wave is when $\frac{4}{\lambda} \text{Re}[(\epsilon_r \mu_r)^{1/2}] = 1$.

C. MATCHING LAYERS FOR PEC BACKING

From Eq. (20), the transcendental equation for matching layers on a PEC backing ($Z_L = 0$) that provides zero specular reflection is

$$Z_{in} - Z_o = 0 \quad (24)$$

or

$$(b) \quad (25)$$

resulting in

$$a, x > 0 \quad (26)$$

where Z_d is given by Eq. (22) and γ by Eq. (12). Substituting in for Z_d and γ , we get

$$\sqrt{\frac{(\mu_r' - j\mu_r'')}{(\epsilon_r' - j\epsilon_r'')}} \tanh\left(jk_o t \sqrt{(\epsilon_r' - j\epsilon_r'')(\mu_r' - j\mu_r'')}\right) - 1 = 0 \quad (27)$$

or

$$j \sqrt{\frac{(\mu_r' - j\mu_r'')}{(\epsilon_r' - j\epsilon_r'')}} \tan\left(\frac{2\pi}{\lambda_o} t \sqrt{(\epsilon_r' - j\epsilon_r'')(\mu_r' - j\mu_r'')}\right) - 1 = 0. \quad (28)$$

It is traditional to use loss tangent for dielectric loss, which is given by

$$\tan \delta_\epsilon = \frac{b}{a}. \quad (29)$$

In terms of the four normalized parameters (Eqs. (15) – (18)), the transcendental equation becomes

$$\sqrt{\frac{x - jy}{a - jb}} \tanh\left(j2\pi \sqrt{(x - jy)(a - jb)}\right) = j \sqrt{\frac{(x - jy)}{(a - jb)}} \tan\left(2\pi \sqrt{(x - jy)(a - jb)}\right) = 1. \quad (30)$$

Note that f_{che} and s_{che} can be positive or negative, but a and b must be positive or zero.

The transcendental equation can be redefined further using two new complex variables

$$v = a - jb \quad (31)$$

and

$$z = x - jy . \quad (32)$$

Now Eq. (30) becomes

$$\sqrt{\frac{z}{v}} \tanh(j2\pi\sqrt{zv}) = j\sqrt{\frac{z}{v}} \tan(2\pi\sqrt{zv}) = 1. \quad (33)$$

The curves on the universal chart (Figure 7) represent combinations of the four parameter groups that satisfy Eq. (33) for DPS material. The universal design chart has curves represented in red and blue lines. The values of a in Eq. (15) are blue, and constant values of Eq. (29) are represented by red lines. Therefore, x and y in Eqs. (17) and (18) can be found by reading the values from the universal design chart on the abscissa and ordinate scales, respectively.

For the left-side curve region along the single curve with material-layer dielectric loss tangent less than 0.3 and $\text{Im}[\mu_r] \geq 3\text{Re}[\mu_r]$, the parameters are approximated by

$$\frac{2\pi t}{\lambda} \text{Im}[\mu_r] = 1 \quad (34)$$

and

$$\text{Re}[\varepsilon] = 3\text{Re}[\mu] . \quad (35)$$

Using the analytic relationship in Eq. (34), we determine the required layer thickness in terms of wavelength and magnetic-permeability imaginary part. Equation (35) determines the relationship between the dielectric constant real parts and magnetic permeability. Equation (35) must be satisfied so as to achieve a reflection result close to zero. It is also important to note that the required thickness is embedded in this equation.

The topside curve region represents matched-characteristic impedance absorbers where $(t/\lambda)\text{Im}[\mu_r] \geq 1$; the parameters are approximated by

$$\text{Re}[\varepsilon_r] = \text{Re}[\mu_r] \quad (36)$$

and

$$\tan \delta_\varepsilon = \tan \delta_\mu \quad (37)$$

where magnetic loss tangent is

$$x \text{ v e r s u s } y . \quad (38)$$

Equations (36) and (37) are defined as matched-characteristic impedance absorbers since both equations are equivalent to a complex statement of real and imaginary part given that $\varepsilon = \mu$. Besides using theory to define the minimum thickness of the material, for practical purposes, the matched-characteristic impedance absorber is equivalent to zero-reflection absorber when $(t/\lambda)\text{Im}[\mu_r] \geq 1$.

The lower-right curve region contains resonant $1/4$ -wavelength absorbers and exhibits a complicated relationship between the four parameter groups, which contribute to a zero-reflection absorber. The lower-right curve consists of two subregions, where the left subregion consists of a contour between $\tan \delta_\varepsilon = 0$ to $\tan \delta_\varepsilon = 0.8$. With the thickness characteristic of $1/4$ wavelength, the lower-right curve can be expressed as

$$\frac{4t}{\lambda} \text{Re}[(\varepsilon_r \mu_r)^{1/2}] = 1 . \quad (39)$$

According to [2], we see that Eq. (39) is most accurate near the $\tan \delta_\varepsilon = 0$ contour. The lower-bottom part of the subregion represents the relationship of $(\pi t/\lambda)\text{Im}(\varepsilon_r) = 1$, where the dielectric loss dominates.

D. SUMMARY

The concept of zero specular reflection was introduced and the governing equations presented in accordance with transmission line theory. Equations for zero specular reflection and matching layers for DPS materials with PEC backing were discussed. A new material diagram in A - B space was introduced. The advantage of the universal design chart is to show the design tradeoffs of a specific dielectric and magnetic materials and the required layer thickness.

In the next chapter, a numerical solution of the transcendental equation is addressed.

IV. SOLUTION RESULTS AND ANALYSIS

In this chapter, the equations discussed in Chapter III are implemented on the four types of lossy MTMs, and their transcendental equations were solved in MATLAB to generate universal curves for various dielectric loss tangents. The solutions are compiled into a set of curves used for evaluation purposes with other MTMs. MATLAB codes are included in Appendix A to Appendix F for reference and discussion.

A. SOLUTION APPROACH

Equation (30) is the transcendental equation that must be satisfied by the parameters a, b, x , and y for zero specular reflection. It applies to any type of passive medium ($b, y \geq 0$). A DPS material has $a, x > 0$, while DNG has $a, x < 0$. A SNG medium has either $a \leq 0$ or $x \leq 0$.

An analytical solution of Eq. (30) is not possible in general (only in some trivial cases). The equation must be solved numerically. The parameters a and b (or equivalently a and $\tan \delta_\varepsilon$) are specified, and then the equation solved for x and y . Note that Eq. (30) is a complex equation and could be separated into two real equations. Some numerical solution packages cannot handle complex variables, in which case two real equations must be solved. However, some software is not capable of solving multiple simultaneous equations.

The MATLAB function *fsolve* and *solve* were used to obtain x and y . *Fsolve* is a function in the optimization toolbox that solves a system of nonlinear equations using iterative techniques. The argument of *fsolve* includes the function name for the equation to be solved. Initial start points must be provided. Upon return, an exitflag identifies the terminal condition of the solution ($-4 \leq \text{exitflag} \leq 4$). There are many options that can be specified. A problem with the iterative solution is that the algorithm may get stuck at a local minimum.

The second MATLAB routine is *solve*, which handles algebraic equations and accepts symbolic expressions or strings. It can solve systems of equations and returns symbolic solutions. The symbolic solutions can be evaluated using *eval*. If symbolic solutions cannot be determined, then *solve* returns numeric solutions.

The MATLAB program was designed for flexibility, allowing the user to enter the dielectric loss tangent, type of MTM, start and end points, and increment in a . The tolerance for convergence is also specified.

In the next sections there are collections of nine dielectric loss tangent curves generated over a search range of a values for each type of MTM. The loss tangent values are 0.01, 0.1, 0.3, 0.5, 0.75, 0.8, 1, 3, and 10, which are similar to [2] so that comparisons can be made.

The remaining user-defined parameters, such as the \tanh tolerance and search range for each curve, were set to remain constant for all cases. The \tanh tolerance was fixed at 10^{-50} , while the start of the search range for DPS was fixed at $x = -0.1$ and $y = -0.1$ and for DNG was fixed at $x = 0$ and $y = 0$.

Once the user has defined the parameters, the MATLAB *fsolve* function is invoked. The returned data is used to generate four plots, as shown in Figure 8. The upper-left plot shows the locus of solutions in x versus y for fixed values of a and b . The upper-right plot shows the complex solution returned from *fsolve*, which is related to x and y . The lower-left plot shows the attenuation α and phase constant β . For the particular case shown in Figure 8 ($\tan \delta_e = 0.3$), we observe that β is positive and conclude that this is a RH medium. The lower-right plot shows the solutions in A - B space. From Figure 5, since A is negative and B positive in this example, the medium is RH and DPS.

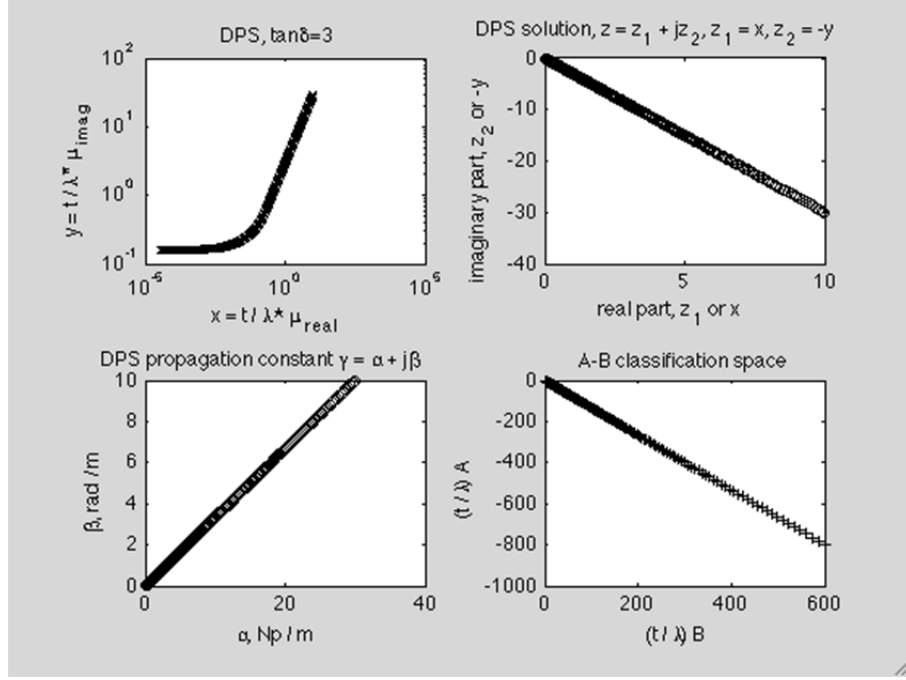


Figure 8. Sample plots generated from the MATLAB program for a DPS medium.

B. MATCHING LAYERS FOR DPS MATERIAL

As cited in Chapter III, Section C, lossy DPS material has both positive real permittivity and permeability. After the four parameter groups were simplified by normalizing a and x by t/λ , the properties of lossy DPS material are such that x and a are positive and y and b are also positive. However the values of y and b are zero when dealing with lossless DPS material. MATLAB's *fsolve* function is used to solve Equation (30) for x and y to generate the DPS curve on the upper left plot in Figure 9. In this DPS example, the dielectric loss tangent of 0.5 was selected. The curves for nine dielectric loss tangents (0.01, 0.1, 0.3, 0.5, 0.75, 0.8, 1, 3, and 10) were generated and combined into one plot as shown in Figure 10.

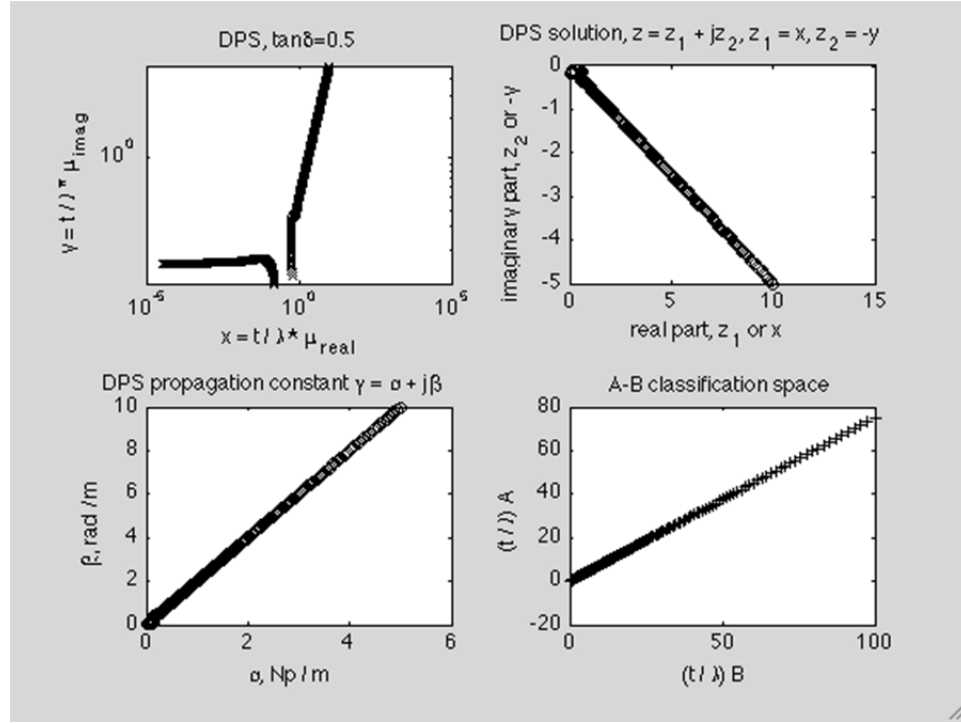


Figure 9. MATLAB generated result on DPS material with $\tan \delta_{\varepsilon} = 0.5$.

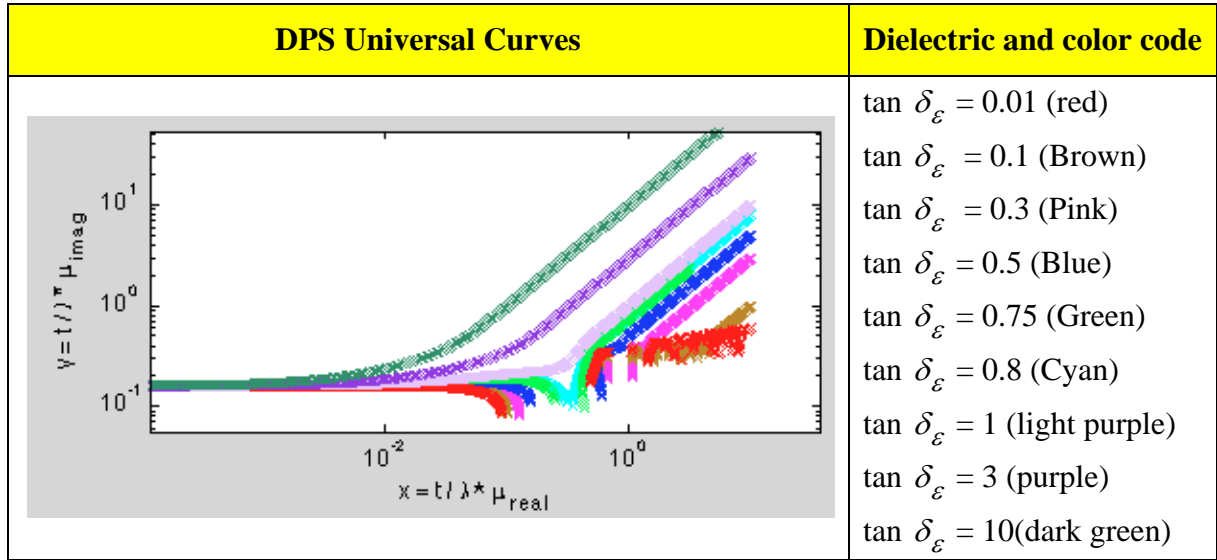


Figure 10. DPS combined universal curves.

A comparison of Figures 7 and 10 shows several differences for small $\tan \delta_\varepsilon$. These differences are a result of convergence problems in *fsolve* and are addressed in Section F of this chapter.

For a DPS material, the normalized permeability parameter is given by z of Eq. (29):

$$z = x - jy. \quad (40)$$

In Figure 11 is shown a plot in the complex plane of the quantity z . In polar form

$$z = |z|e^{-j\phi_z} \quad (41)$$

where

$$\phi_z = \tan^{-1}(y/x). \quad (42)$$

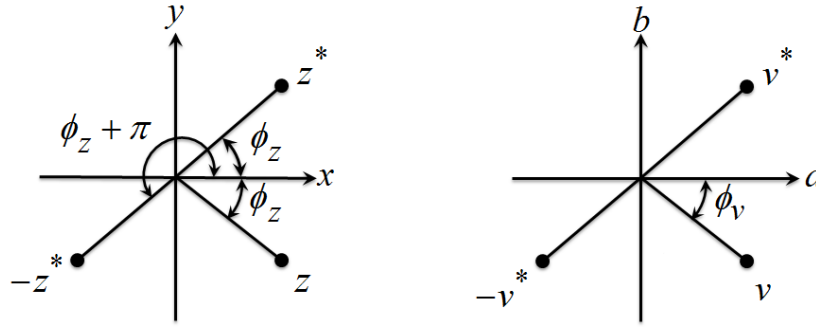


Figure 11. Plots of the variables z and v in the complex plane.

In polar form, the complex permittivity parameter of Eq. (31) is

$$v = |v|e^{-j\phi_v} \quad (43)$$

where

$$\phi_v = \tan^{-1}(b/a). \quad (44)$$

Therefore, the square root of the product of z and v is

$$\sqrt{zv} = \sqrt{|z||v|} e^{-j\phi_z/2} e^{-j\phi_v/2} \quad (45)$$

$$= \sqrt{|z||v|} e^{-j(\phi_z + \phi_v)/2}. \quad (46)$$

From the argument of the \tanh function in Eq. (33),

$$\pm\gamma t = \pm(\alpha + j\beta)t = \pm j2\pi\sqrt{vz} \quad (47)$$

$$= \pm j2\pi\sqrt{|v||z|} e^{-j\Phi^+} \quad (48)$$

$$= \pm j2\pi\sqrt{|v||z|} (\cos \Phi^+ - j \sin \Phi^+) \quad (49)$$

$$= \pm 2\pi\sqrt{|v||z|} (\sin \Phi^+ + j \cos \Phi^+) \quad (50)$$

where

$$\Phi^+ \equiv (\phi_v + \phi_z)/2 \text{ and } 0 \leq \Phi^+ \leq \pi/2. \quad (51)$$

Therefore, we conclude that a positive sign must be selected to achieve α positive. This selection of the positive sign gives a positive β , which is a RH medium.

The lower right plot of Figure 9 was generated to show the solutions in A - B space of Lee and Park [6]. For a DPS material, the two parameters of A and B are

$$A = \left(\frac{t}{\lambda}\right)^2 (\varepsilon'_r \mu'_r - \mu''_r \varepsilon''_r) = ax - by \quad (52)$$

and

$$B = \left(\frac{t}{\lambda}\right)^2 (\varepsilon'_r \mu''_r + \mu'_r \varepsilon''_r) = ay + bx. \quad (53)$$

From Figure 9, A and B are positive, which is a DPS RH material from Figure 5.

C. MATCHING LAYERS FOR DNG MATERIAL

As cited in Chapter III, Section C, lossy DNG material has both negative real permittivity and permeability with non-zero imaginary parts. After the four parameter groups were simplified by normalizing by t/λ , the properties of lossy DNG material are such that a and x are negative and b and y are positive. For the DNG case, Eq. (30) becomes

$$j \sqrt{\frac{(-x - jy)}{(-a - jb)}} \tan \left(\underbrace{2\pi \sqrt{(-x - jy)(-a - jb)}}_{\equiv \gamma t / j} \right) = 1. \quad (54)$$

MATLAB's *fsolve* function is used to solve Eq. (30) for $\tan \delta_\epsilon = 0.5$ and generate the DNG curves in Figure 12. Similar to the DPS case, nine dielectric loss tangents were used to generate the combined curves shown in Figure 13.

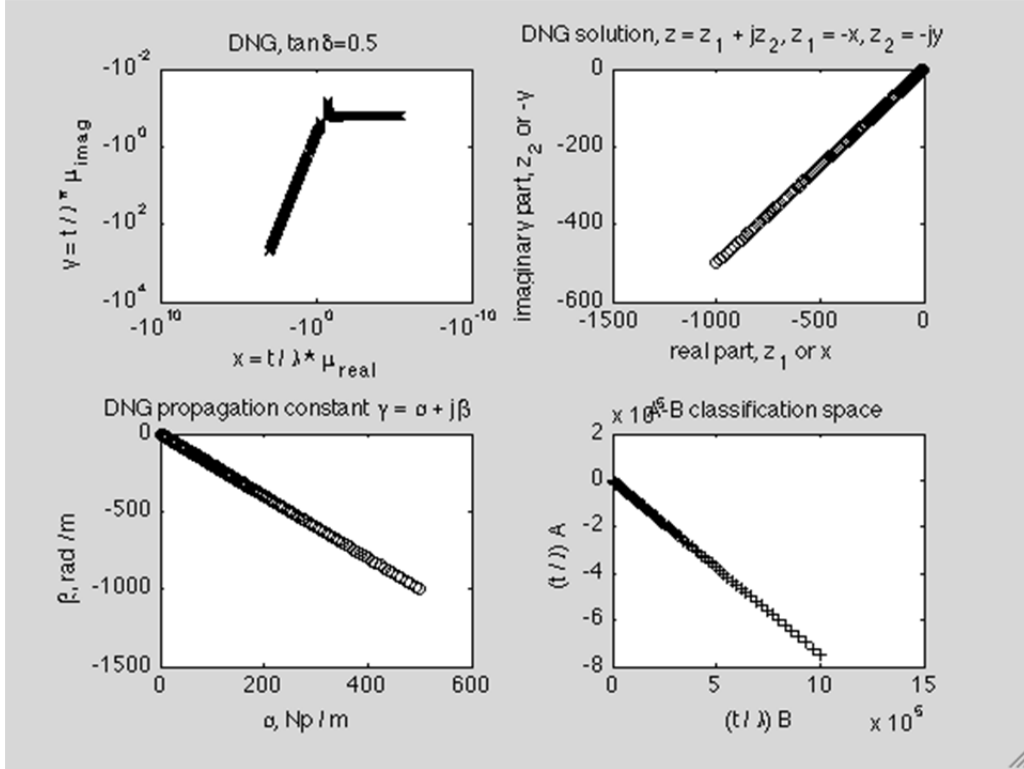


Figure 12. MATLAB generated result for DNG material with $\tan \delta_\epsilon = 0.5$.

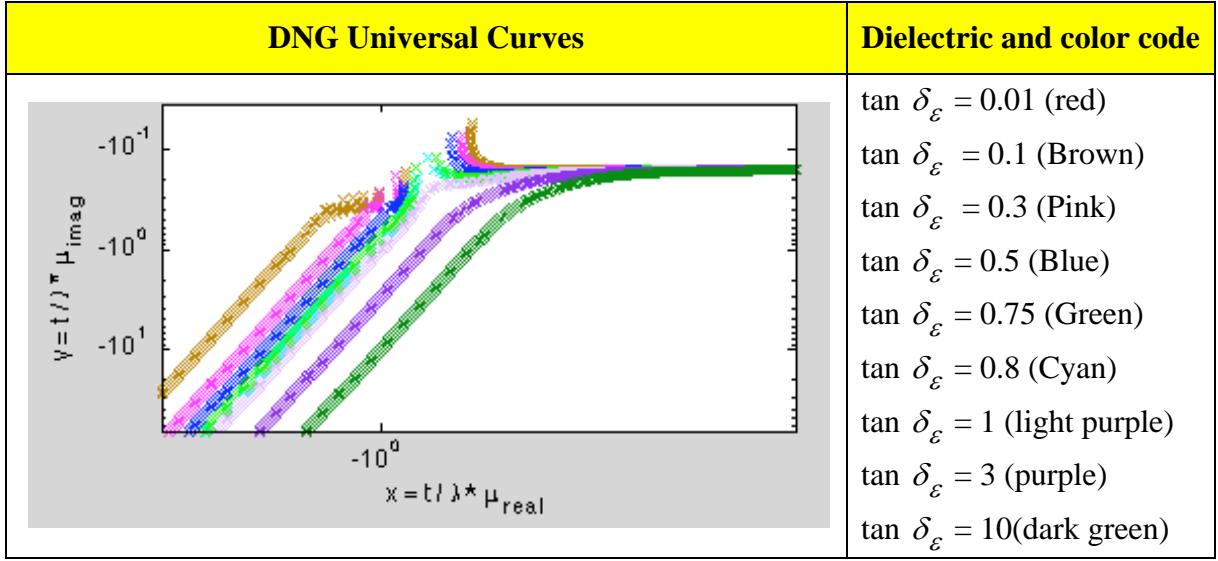


Figure 13. DNG combined universal curves.

In terms of v and z in Eqs. (31) and (32), Eq. (54) can be redefined as

$$\sqrt{\frac{-z^*}{-v^*}} \tanh\left(j2\pi\sqrt{(-z^*)(-v^*)}\right) = j\sqrt{\frac{-z^*}{-v^*}} \tan\left(2\pi\sqrt{(-z^*)(-v^*)}\right) = 1. \quad (55)$$

Using the properties of complex numbers, we can write Eq. (55) as

$$j\sqrt{\frac{z}{v}} \tan\left(-2\pi\sqrt{(z)(v)^*}\right) = 1 \quad (56)$$

or

$$-j\sqrt{\frac{z}{v}} \tan\left(2\pi\sqrt{vz}\right)^* = 1. \quad (57)$$

Shown previously in Figure 11 is a plot in the complex plane of the quantity $-z^*$. In polar form

$$-z^* = |z|e^{j(\phi_z + \pi)} \quad (58)$$

where ϕ_z is defined in Eq. (42). Similarly,

$$-v^* = |v| e^{j(\phi_v + \pi)} \quad (59)$$

where ϕ_v is defined in Eq. (44).

The square root of the product of $-z^*$ and $-v^*$ is

$$\sqrt{(-z^*)(-v^*)} = \sqrt{|z||v|} e^{j(\phi_z + \pi)/2} e^{j(\phi_v + \pi)/2} \quad (60)$$

or

$$\sqrt{zv}^* = -\sqrt{|z||v|} e^{j(\phi_z + \phi_v)/2}. \quad (61)$$

For the leading square root factor in Eq. (55), we note that

$$\sqrt{\frac{-z^*}{-v^*}} = \sqrt{\frac{|z|}{|v|}} e^{j(\phi_z + \pi)/2} e^{-j(\phi_v + \pi)/2} \quad (62)$$

and

$$\sqrt{\frac{|z|}{|v|}} e^{-j(\phi_z - \phi_v)/2} = \sqrt{\frac{|z|}{|v|}}^* \quad (63)$$

For DNG material, the argument of the \tanh is

$$\gamma t = (\alpha + j\beta)t = \pm j2\pi\sqrt{vz}^* \quad (64)$$

$$= \pm j2\pi\sqrt{|v||z|} e^{j\Phi^+} \quad (65)$$

$$= \pm j2\pi\sqrt{|v||z|} \left(\cos \Phi^+ + j \sin \Phi^+ \right) \quad (66)$$

where Φ^+ is defined in Eq. (51).

Therefore, we conclude that in order to achieve α positive, the negative sign of the square root must be selected. Thus,

$$(\alpha + j\beta)t = 2\pi\sqrt{|v||z|} \left(-j \cos \Phi^+ + \sin \Phi^+ \right). \quad (67)$$

The lower left of Figure 12 consists of a plot of α vs. β . It is seen that $\alpha \geq 0$ and the phase constant $\beta < 0$, signifying that this is LH material.

The lower right of Figure 12 contains a plot of the solutions in A - B space of Lee and Park [6]. The two parameters of A and B for DNG are

$$A = \left(\frac{t}{\lambda} \right)^2 (\epsilon'_r \mu'_r - \mu''_r \epsilon''_r) = ax - by \quad (68)$$

and

$$B = \left(\frac{t}{\lambda} \right)^2 (\epsilon'_r \mu''_r + \mu'_r \epsilon''_r) = -ay - bx. \quad (69)$$

Using the material classifications in Figure 5, we determine that this type of material LH, since $B \leq 0$ always.

By comparing the DPS and DNG simulation results, we observed there is a relationship between the two solutions, which results in a symmetry that is apparent in Figure 10 and Figure 13. The simulation results were further verified by comparing both DPS and DNG equations. The mathematical results show that the DPS case in Eq. (33) is the complex conjugate of the DNG case in Eq. (57). Therefore, we conclude that if z is the solution to Eq. (33) for a given v , then for the DNG case, $-z^*$ is the solution to Eq. (55) for $-v^*$.

D. MATCHING LAYERS FOR ENG MATERIAL

As cited in Chapter III, Section C, ENG material has $\varepsilon'_r < 0$ and $\mu'_r > 0$. With regard to the normalized parameters in Eqs. (15) – (18), the properties of lossy ENG material are such that x is negative and a, b and y are positive. Equation (30) adapted for ENG becomes

$$\pm \sqrt{\frac{x - jy}{-a - jb}} \tanh\left(\pm j2\pi\sqrt{(x - jy)(-a - jb)}\right) = 1. \quad (70)$$

In terms of z in Eq. (32) and the complex permittivity parameter v in Eq. (31), Eq. (70) can be written as

$$\pm \sqrt{\frac{z}{-v^*}} \tanh\left(\pm j2\pi\sqrt{(z)(-v^*)}\right) = \pm j \sqrt{\frac{z}{-v^*}} \tan\left(\pm 2\pi\sqrt{(z)(-v^*)}\right) = 1. \quad (71)$$

The square root of the product of z and $-v^*$ (both shown in the complex plane in Figure 11) is

$$\sqrt{z(-v)^*} = \sqrt{|z||v|} e^{j\phi_v/2} e^{-j\phi_z/2} \quad (72)$$

$$= \sqrt{|z||v|} e^{-j\Phi^-} \quad (73)$$

where

$$\Phi^- = \frac{\phi_z - \phi_v}{2} \text{ and } \frac{-\pi}{4} \leq \Phi^- \leq \frac{\pi}{4}. \quad (74)$$

For ENG material, the argument of the \tanh is

$$(\alpha + j\beta)t = \pm j2\pi\sqrt{|v||z|} e^{-j\Phi^-} \quad (75)$$

$$= \pm j2\pi\sqrt{|v||z|} \left(-\cos \Phi^- - j \sin \Phi^-\right) \quad (76)$$

$$= 2\pi\sqrt{|v||z|} \left(\cos \Phi^- - j \sin \Phi^- \right). \quad (77)$$

Therefore, we conclude that in order to achieve α positive, the sign in the ENG case has to be positive.

The leading square root factor in Eq. (70) is a scaled complex impedance. In terms of the complex variables z and v

$$Z = R + jX = \pm \sqrt{\frac{x - jy}{-a - jb}} = \pm \sqrt{\frac{z}{-v^*}} \quad (78)$$

$$= \pm (-j) \sqrt{\frac{|z|}{|v|}} e^{-j\Phi^+} \quad (79)$$

$$= \pm \sqrt{\frac{|z|}{|v|}} \left[-j \cos \Phi^+ - \sin \Phi^+ \right] \quad (80)$$

where

$$0 \leq \Phi^+ \leq \frac{\pi}{2}. \quad (81)$$

For a passive medium $R \geq 0$, so the negative sign must be used. This choice results in a positive reactance (X), so this impedance is inductive.

The two parameters A and B for ENG are

$$A = \left(\frac{t}{\lambda} \right)^2 \left(-\varepsilon'_r \mu'_r - \mu''_r \varepsilon''_r \right) = -ax - by \quad (82)$$

and

$$B = \left(\frac{t}{\lambda} \right)^2 \left(-\varepsilon'_r \mu''_r + \mu'_r \varepsilon''_r \right) = -ay + bx. \quad (83)$$

Using the material classifications in Figure 5, we see that this type of material can be RH or LH, depending on the sign of B .

E. MATCHING LAYERS FOR MNG MATERIAL

As cited in Chapter III, Section C, MNG material has $\varepsilon'_r > 0$ and $\mu'_r < 0$. With regard to the normalized parameters in Eqs. (15) – (18), the properties of lossy MNG material are such that a is negative and b, x and y are positive. Equation (30) adapted for MNG becomes

$$j \sqrt{\frac{(-x - jy)}{(a - jb)}} \tan \left(\underbrace{\sqrt{(-x - jy)(a - jb)}}_{\equiv \gamma t / j} \right) = 1. \quad (84)$$

Using the complex permittivity and permeability parameters z and v , we can write Eq. (84) as

$$\pm \sqrt{\frac{-z^*}{v}} \tanh \left(\pm j 2\pi \sqrt{(-z^*)(v)} \right) = \pm j \sqrt{\frac{-z^*}{v}} \tan \left(2\pi \sqrt{(-z^*)(v)} \right) = 1. \quad (85)$$

The square root of the product of v and $-z^*$ is

$$\sqrt{v(-z)^*} = \sqrt{|z||v|} e^{-j\phi_v/2} e^{j\phi_z/2} \quad (86)$$

$$= \sqrt{|z||v|} e^{-j\Phi^-}. \quad (87)$$

For MNG material, the argument of the \tanh is

$$(\alpha + j\beta)t = \pm j 2\pi(j) \sqrt{|v||z|} e^{-j\phi_v/2} e^{j\phi_z/2} \quad (88)$$

$$= 2\pi \sqrt{|v||z|} \left(\cos \Phi^- - j \sin \Phi^- \right) \quad (89)$$

where Φ^- is defined in Eq. (74). Therefore, we conclude that in order to achieve α being positive, the selected sign in the MNG case has to be positive. Then the sign of β depends on whether $\sin \Phi^-$ is positive or negative.

The leading impedance factor in Eq. (85) is

$$Z = R + jX = \pm \sqrt{\frac{-z^*}{v}} = \pm (j) \sqrt{\frac{|z|}{|v|}} e^{j\Phi^+} \quad (90)$$

$$= \pm \sqrt{\frac{|z|}{|v|}} \left[j \cos \Phi^+ - \sin \Phi^+ \right] \quad (91)$$

where

$$0 \leq \Phi^+ \leq \frac{\pi}{2}. \quad (92)$$

To obtain a positive resistance the negative sign is selected. The reactance X is negative, which is capacitive.

The two parameters of Lee and Park are

$$A = \left(\frac{t}{\lambda} \right)^2 \left(-\varepsilon'_r \mu'_r - \mu''_r \varepsilon''_r \right) = -ax - by \quad (93)$$

and

$$B = \left(\frac{t}{\lambda} \right)^2 \left(-\varepsilon'_r \mu''_r + \mu'_r \varepsilon''_r \right) = ay - bx. \quad (94)$$

Using the material classifications in Figure 5, we see that this type of material can be RH or LH, depending on the sign of B .

F. NUMERICAL SOLUTION FOR ENG AND MNG

Numerical solutions for the ENG and MNG equations were programmed in MATLAB. The *fsolve* function was called to obtain solutions x and y for a range of a and b , subject to the constraints $\alpha \geq 0$ and $R \geq 0$. *Fsolve* was not able to obtain solutions to either the ENG or MNG equation. It returned only values that would result in a DNG or DPS material. For example, the ENG equation, for which we expect $x > 0$ when $a < 0$, returned $x < 0$. Similarly, the MNG equation, which should have $x < 0$ when

$a > 0$, returned values of $x > 0$. Several programming variations were tried, all with the same results.

The numerical algorithms indicate that there are no ENG or MNG materials that provide zero specular reflection, yet satisfy $\alpha \geq 0$ and $R \geq 0$. There are reports in the literature that allude to this fact. Reference [13] found that it was necessary to pair a ENG layer with a MNG layer to obtain zero reflection. This result is not readily evident from the equations, although it should be possible to verify by mathematical proof.

G. DISCUSSION OF SOLUTION METHODS

The transcendental equations were programmed into MATLAB with flexibility for the user to define the search area of interest and the type of material and its parameters. In this section, the DPS results are compared with curves obtained from published data [2]. There are no previously published curves for the DNG, ENG and MNG cases. However, from the symmetry of the transcendental equations, some relationships to the DPS case can be inferred. The universal curves for the DPS and DNG cases were shown in Figures 10 and 13.

We expect that for DPS parameters we would be able to achieve curves similar to those in [2]. During the process of generating the curves for some dielectric loss tangents, it was found that the form of the transcendental equation using “tanh” produces incomplete curves with gaps in-between. The results improved after changing the equation to the “tan” form. To ensure that numerical round off was not a problem, the number of digits used by MATLAB was set to 32 and 64. This setting had no observable effect on the results, but 64 digits were used for all solutions.

A *fsolve* tolerance value of 10^{-50} was specified. The search start values provided to *fsolve* were adjusted depending on the range of a for both x and y . The results show that some portions of the curves may be missing if improper initial points are given; for example, if solutions for $0.1 \leq a \leq 1$ are requested and a start point of 10 is given. Figure 14 was generated for $\tan \delta_e = 0.01$ using 1000 values of a between 10^{-5} and 10^3 with an

initial search range of $x = 0$ and $y = 0$. Figure 14 is inconsistent with the characteristics expected for the solution and indicate *fsolve* is not converging to a solution. The exitflag value returned by *fsolve* echoes this warning for many of the points returned. Another problem was the inability to obtain solutions that have very small values of y (i.e. at the bottom of the chart).

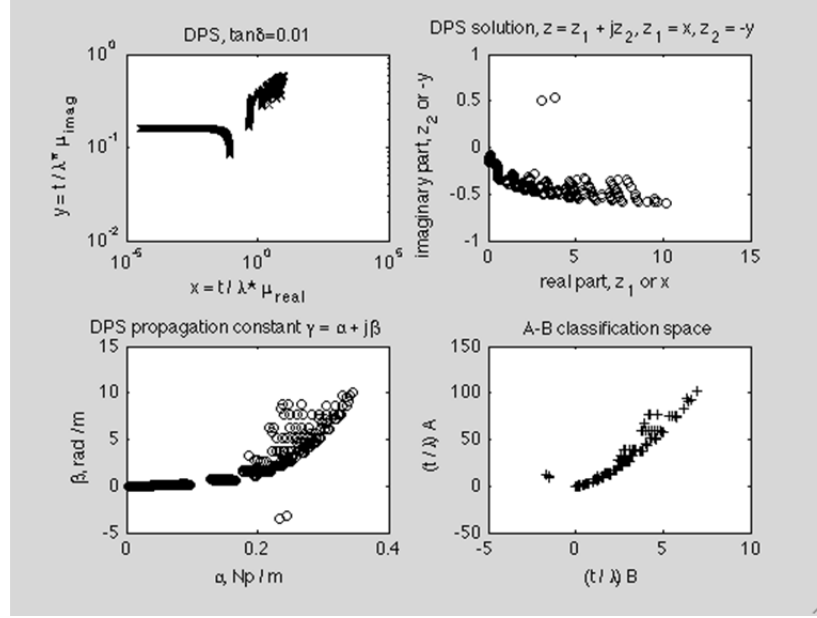


Figure 14. *fsolve* solutions for a DPS material with $\tan \delta_{\varepsilon} = 0.01$, search start points of $x=10^{-4}$ and $y=10^1$.

Figure 15 is the same case as in Figure 14 but uses different initial search points and more curve points to obtain greater detail. The result shows that there are hook-like features in the curve in the top left plot.

A modified version of the program, shown in Appendix G, re-solves the equation for a range of a using initial estimates that are selected based on the region of the chart. A set of solutions for $\tan \delta_{\varepsilon}=0.3$ is shown in Figure 16. The parameters are set according to Table 3, and the colors represent different initial x and y values as shown in Table 4. The result shows that there is a completely new curve as compared to published data [2]. We concluded that this fictitious curve is a numerical artifact of *fsolve*.

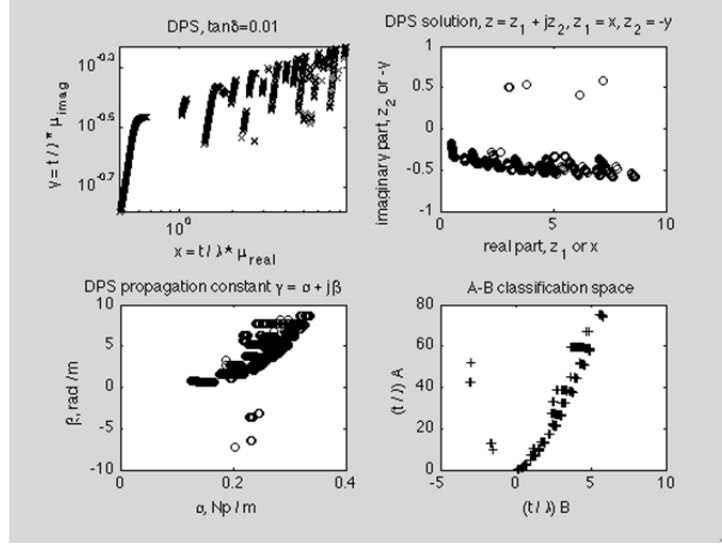


Figure 15. *fsolve* solutions for a DPS material with $\tan \delta_{\varepsilon} = 0.01$, search start points of $x=10^{-0.35}$ and $y=10^{0.95}$.

Table 3. Parameters for the modified MATLAB program for variable initial points.

Parameters	Settings
Type of material	DPS
Dielectric loss tangent	0.3
Start and end search of A values	Start search = $-2 \left(10^{-2}\right)$ End search = $1 \left(10^1\right)$
Search value points	1000 points
Start of search range	$x = 0.1$ and $y = 0.01$
<i>fsolve</i> tolerance	10^{-4}

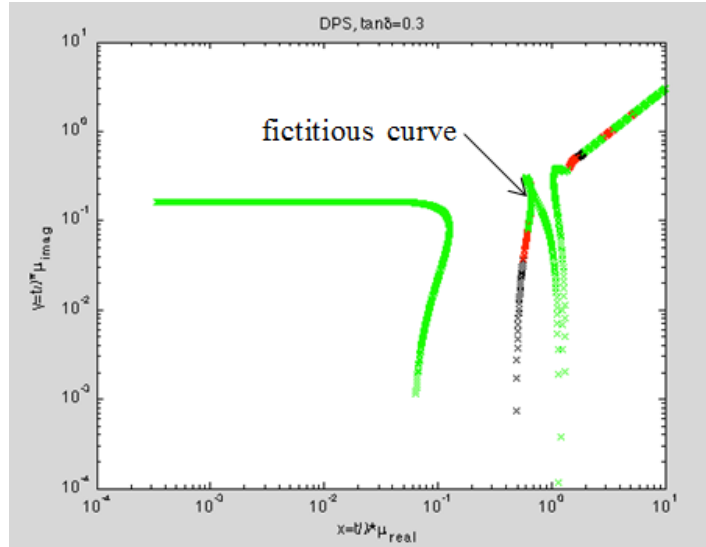


Figure 16. A curve generated for DPS material by solving the equation three times each with different initial start points.

Table 4. Color code for the results in Figure 16.

Parameters	Array of estimates		
Start of search range	$x = 0.5$ and $y = 0.01$	$x = 0.75$ and $y = 0.01$	$x = 1$ and $y = 0.01$
Color Code	black	red	green

In reference [2], there is no mention of the algorithm used to solve the equations and generate the curves. In order to validate the data, solutions were generated for several cases using another MATLAB function named *solve*. The MATLAB code was programmed as shown in Appendix H. The transcendental equation and all of parameters must be converted to a string. The program has a setting for the number of digits converted to a string by using the function “num2str”, which converts numbers to strings. In Figure 17 the settings for num2str are blue for ten and red for twenty-four. The results were generally better with more digits, however, for large numbers like sixty-four, the program could not find a solution for the requested tolerance.

A frequent problem with *solve* is that the program encountered “no solution found” and MATLAB had a core fault. Some memory would be corrupted, which required restarting MATLAB.

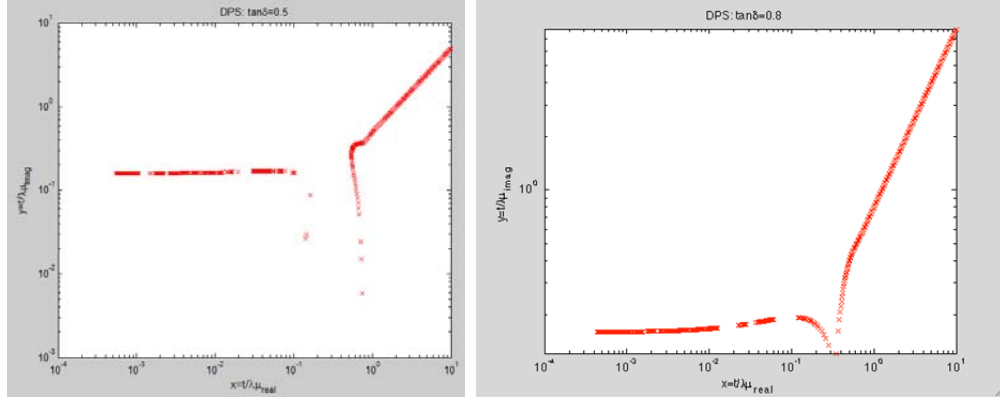


Figure 17. Curves generated using the *solve* function; $\tan \delta_\varepsilon = 0.5$ (left) and $\tan \delta_\varepsilon = 0.8$ (right).

By comparing *fsolve* and *solve* function results, we observed that both functions generate similar curves, for example, as shown in Figure 18. The advantage of *fsolve* is the ability to generate the curves using iterative technique to solve the nonlinear equations, which proves to generate the better resolution curves. The time taken for *fsolve* function to generate the curves is much shorter than *solve*; *fsolve* uses less than a min to generate 1000 points while *solve* function uses about 20 mins to generate 500 points.

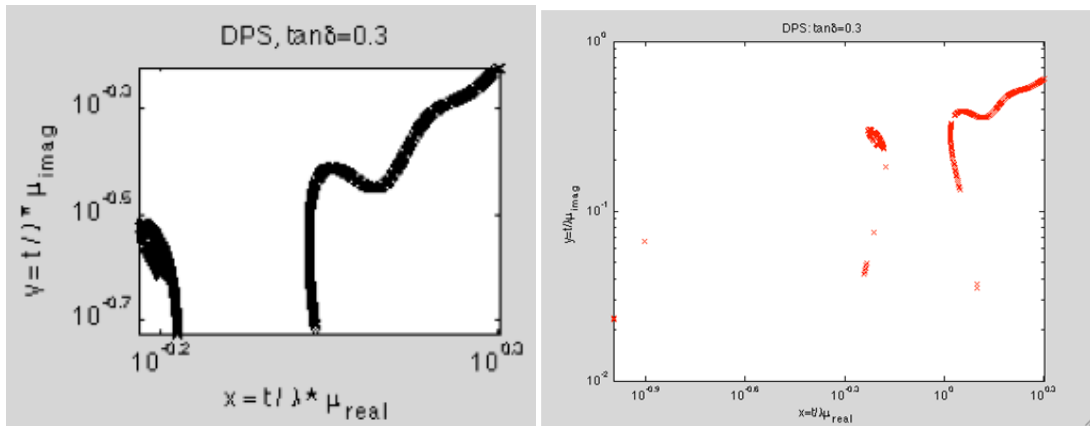


Figure 18. Simulation result generated using *fsolve* (left) and *solve* (right) function.

H. SUMMARY

In this chapter, the specific equations for each of the four types of metamaterial were presented. The numerical solution programs and output plots with the results were shown. The parameters used to generate the results were also discussed in relation to the A - B space for lossy materials defined in [2]. The program was able to solve the numerical equations and generate the plots of the universal design curves for DPS and DNG materials for most areas of the chart.

However, the MATLAB functions *fsolve* and *solve* apparently had some problems with the iterative solution in that the algorithm may get stuck at a local minimum. The numerical algorithms indicated that physical solutions to the ENG and MNG equations do not exist.

V. CONCLUSION

A. SUMMARY AND CONCLUSION

The platform radar signature or radar cross section is one of the critical considerations in modern warfare and often RAM is applied to reduce RCS to increase survivability. To overcome the disadvantages of RAM such as heavy weight, bulkiness, high cost, etc, the unique properties of MTM were investigated to achieve near zero specular reflection for low RCS applications.

An introduction of MTM theory and characteristics were discussed. The general propagation constant and the material diagram in A - B space for lossy MTMs and the relationship to their handedness were discussed. An important note is that the sign of B defines the material handedness, RH or LH. The material is RH when $B > 0$ and LH when $B < 0$. However, the sign of A can be either positive or negative for both DPS and DNG but has to be negative for both ENG and MNG.

The transcendental equations related to zero specular reflection were derived based on transmission line theory. The transcendental equation was specialized for the four types of MTM matching layers to produce zero specular reflection of a layer with PEC backing. The transcendental equations were solved numerically using the MATLAB *fsolve* and *solve* functions in order to generate universal curves. The DPS curves show similar results as compared to published data [2] except for small value of y . This is attributed to non-convergence of the numerical solution algorithms. The results verify that the DNG equation is the complex conjugate of the DPS equation. Therefore, one set of curves can be used for both DPS and DNG cases if the proper substitution of signs is made for a , b , x and y . The numerical algorithm indicated that there are no physical solutions to the ENG and MNG equations. It should be possible to verify this result by mathematical proof.

The generated curves for different MTMs can be used to design a matched-surface RAM for military applications. The curves show that only two types of materials (DPS and DNG) can provide zero specular reflection. Even though the EM propagation

characteristics change in the various MTMs, the important end result is that zero specular reflection can be achieved. In principle, such materials allow an object to cloak itself to create “invisibility” to a radar.

B. FUTURE WORK

In this thesis, two MATLAB functions, *fsolve* and *solve* were employed to generate curves for four types of MTMs. As discussed, there are some discrepancies in the results between the generated curves and published data [2]. Therefore, future research should delve into the source of the error and search for potential remedies. Other software packages such as MATHEMATICA and MATHCAD have equation solvers. MATHCAD was used to generate the curves in Figure 7 without any noticeable convergence problems. It would be beneficial to use the MATHCAD routine to solve the DNG, ENG and MNG cases for comparison. The results obtained could be used to conduct simulations in Microwave Studio (MWS) in order to determine reflection and transmission properties of any given model.

Another direction of research is to re-examine the transcendental equations for ENG and MNG and verify that there is no solution for the given constraints. Furthermore, the equations can be modified to account for non-normal incidence angle and other backing materials.

From [13] and [14], the plane wave interaction with a pair of ENG-MNG slabs would, under certain conditions, lead to some unusual features such as resonance, zero reflection, complete tunneling and transparency. The reflection and transmission results show that the flow of the Poynting vector within the structures, under zero-reflection conditions was satisfied. Therefore, even though individual SNG surfaces cannot provide zero specular reflection, a combined layer of ENG and MNG can.

Finally, the regions on the chart need to be connected to realizable MTMs. For example, given a frequency band and thickness of interest (t/λ), what areas of the chart could SRRs be used as inclusions?

APPENDIX

A. MATLAB CODE FOR UNIVERSAL DESIGN CHART USING FSOLVE FUNCTION

[illegible]

```

[z fval]=fsolve(@(X) transcend_DPS_PEC_pos(X,a,b), [x_est; y_est],...
optimset('TolFun',Tol,'Display','off'));
    % TolFun = Termination tolerance on x,
    % positive scalar with default value 1e-6
    % 'off' displays no output

% save values for check
x(n)=z(1);          % x = Z1
y(n)=-z(2);         % y = Z2
W(n)=x(n)-j*y(n);   % w(n)= x - jy(n)
zz(n)=z(1)+j*z(2);  % z = z1 + jz2
Z(n)=sqrt(zz(n)/(a-j*b)); % z(n) = sqrt((z(1)+jz(2))/(a-jb))
G=sqrt((a-j*b)*zz(n)); % G = sqrt((a-jb)(z1+jz2))

% choose solution with positive alpha
Gam(n)=G*j;
if real(Gam(n))<0, Gam(n)=-Gam(n); end    % alpha > 0 always

% A and B parameters
AA(n)=x(n)*a-y(n)*b;
BB(n)=y(n)*a+b*x(n);
end
close(hwait);
figure(11)
clf

subplot(221)
loglog(x,y,'xk')
xlabel('x = t / \lambda * \mu_{re_a_l}')
ylabel('y = t / \lambda * \mu_{im_a_g}')
title([num2str(SOL),', tan\delta=',num2str(tandel)])

subplot(222)
plot(real(zz),imag(zz),'ko')
title([num2str(SOL),' solution, z = z_1 + jz_2, z_1 = x, z_2 = -jy'])
xlabel('real part, z_1 or x')
ylabel('imaginary part, z_2 or -y')

subplot(223)
plot(real(Gam),imag(Gam),'ko')
title([num2str(SOL),' propagation constant \gamma = \alpha + j\beta'])
xlabel('\alpha, Np / m')
ylabel('\beta, rad / m')
subplot(224)
plot(BB,AA,'k+')

```

```

title('A-B classification space')
ylabel('(t / \lambda) A')
xlabel('(t / \lambda) B')
Lmax=floor(max([max(abs(AA)),max(abs(BB))]))+1;

end    % end of DPS block

%%%%%%%%%%%%%%%%%%%%%%%%%%%%%%%%%%%%%%%%%%%%%%%%%%%%%%%%%%%%%%%%%%%%%%%%%%%%%%
%%%DNG%%%DNG%%%DNG%%%DNG%%%DNG%%%
%%%%%%%%%%%%%%%%%%%%%%%%%%%%%%%%%%%%%%%%%%%%%%%%%%%%%%%%%%%%%%%%%%%%%%%%%%%%%%
% solution for DNG case
if SOL=='DNG'
    for n=1:N
        waitbar(n/N,hwait);
        a=A(n);
        b=B(n);
        [z fval]=fsolve(@(X) transcend_DNG_PEC_neg(X,a,b), [x_est; y_est],...
            optimset('TolFun',Tol,'Display','off'));

% save values for check
        x(n)=-z(1);           % x = -Z1
        y(n)=-z(2);           % y = -Z2
        W(n)=-x(n)-j*y(n);    % both x and y are negative % w(n)= -x - jy(n)
        zz(n)=-z(1)-j*z(2);   % solution to equation % z = -z1 - jz2
        Z(n)=sqrt(zz(n)/(-a-j*b)); % z(n) = sqrt((-z(1)-jz(2))/(-a-jb))
        if real(Z(n))<0, Z(n)=-Z(n); end
        G=sqrt(zz(n)*(-a-j*b)); % G = sqrt((-a-jb)(z1+jz2)

% choose solution with positive alpha
        Gam(n)=G*j;
        if real(Gam(n))<0, Gam(n)=-Gam(n); end    % alpha > 0 always

% A and B parameters
        AA(n)=x(n)*a-y(n)*b;    % for new solution x<0 for DNG
        BB(n)=-y(n)*a-b*x(n);
    end

close(hwait);
figure(12)
clf

subplot(221)
loglog(x,y,'xk')
xlabel('x = t / \lambda * \mu_{r_e_a_l}')
ylabel('y = t / \lambda * \mu_{i_m_a_g}')

```

```

title([num2str(SOL),', tan\delta=',num2str(tandel)])
subplot(222)
plot(real(zz),imag(zz),'ko')
title([num2str(SOL),', solution, z = -z_1 - jz_2, z_1 = -x, z_2 = -jy'])
xlabel('real part, z_1 or x')
ylabel('imaginary part, z_2 or -y')

subplot(223)
plot(real(Gam),imag(Gam),'ko')
title([num2str(SOL),', propagation constant \gamma = \alpha + j\beta'])
xlabel('\alpha, Np / m')
ylabel('\beta, rad / m')

subplot(224)
plot(BB,AA,'k+')
title('A-B classification space')
ylabel('(t / \lambda) A')
xlabel('(t / \lambda) B')
Lmax=floor(max([max(abs(AA)),max(abs(BB))]))+1;

end    % end of DNG block

%%%%%%%%%%%%%%%%%%%%%%%%%%%%%%%%%%%%%%%%%%%%%%%%%%%%%%%%%%%%%%%%%%%%%%%%%%%%%%
% solution for MNG case
if SOL=='MNG'
    for n=1:N
        waitbar(n/N,hwait);

% a and b are the negative of these values in the transcendental equation
a=A(n);
b=B(n);
[z fval]=fsolve(@(X) transcend_MNG_PEC_neg(X,a,b), [x_est; y_est],...
    optimset('TolFun',Tol,'Display','off'));

% save values for check
x(n)=-z(1);          % x = -Z1
y(n)=-z(2);          % y = -Z2
W(n)=-x(n)-j*y(n);   % both x and y are negative % w(n)= -x - jy(n)
zz(n)=-z(1)-j*z(2);  % solution to equation % z = -z1 - jz2
Z(n)=sqrt(zz(n)/(a-j*b)); % z(n) = sqrt((-z(1)-jz(2))/(-a-jb))
if real(Z(n))<0, Z(n)=-Z(n); end
G=sqrt(zz(n)*(a-j*b)); % G = sqrt((-a-jb)(-z1-jz2)

```

```

% choose solution with positive alpha
    Gam(n)=G*j;
    if real(Gam(n))<0, Gam(n)=-Gam(n); end % alpha > 0 always

% A and B parameters
    AA(n)=-x(n)*a-y(n)*b; % for new solution x<0 for MNG
    BB(n)=y(n)*a-b*x(n);
end
close(hwait);

figure(13)
clf
subplot(221)
loglog(x,y,'xk')
xlabel('x=t\lambda*\mu_{real}')
ylabel('y=t\lambda*\mu_{imag}')
title([num2str(SOL), ' \tan\delta=', num2str(tandel)])

subplot(222)
plot(real(zz),imag(zz),'ko')
title([num2str(SOL), ' solution, z=z_1+jz_2, z_1=-x, z_2=-jy'])
xlabel('real part, z_1 or -x')
ylabel('imaginary part, z_2 or -y')

subplot(223)
plot(real(Gam),imag(Gam),'ko')
title([num2str(SOL), ' propagation constant \gamma=\alpha+j\beta'])
xlabel('\alpha, Np/m')
ylabel('\beta, rad/m')

subplot(224)
plot(BB,AA,'k+')
title('A-B classification space')
ylabel('(t\lambda) A')
xlabel('(t\lambda) B')
Lmax=floor(max([max(abs(AA)),max(abs(BB))]))+1;

end % end of MNG block

```



```

%%%%%%%%%%%%%%%%%%%%%%%%%%%%%%%%%%%%%%%%%%%%%%%%%%%%%%%%%%%%%%%%%%%%%%%%
%%%ENG%%%%%%%%%%%%%%%%%%%%%%%%%%%%%%%%%%%%%%%%%%%%%%%%%%%%%%%%%%%%%%%%%%%%%%%%ENG%%%%%%%%%%%%%%%%%%%%%%%%%%%%%%%%%%%%%%%%%%%%%%%%%%%%%%%%%%%%%%%%%%%%%%%%ENG%%%
%%%%%%%%%%%%%%%%%%%%%%%%%%%%%%%%%%%%%%%%%%%%%%%%%%%%%%%%%%%%%%%%%%%%%%%%
% solution for ENG case
if SOL=='ENG'
    for n=1:N
        waitbar(n/N,hwait);

% a and b are the negative of these values in the transcendental equation
        a=A(n);
        b=B(n);
        [z fval]=fsolve(@(X) transcend_ENG_PEC_neg(X,a,b), [x_est; y_est],...
            optimset('TolFun',Tol,'Display','off'));

% save values for check
        x(n)=z(1);           % x = Z1
        y(n)=z(2);           % y = Z2
        W(n)=x(n)-j*y(n);     % x is positive
        zz(n)=z(1)+j*z(2);     % solution to equation
        Z(n)=sqrt(zz(n)/(-a-j*b));
        if real(Z(n))<0, Z(n)=-Z(n); end
        G=sqrt(zz(n)*(-a-j*b));

% choose solution with positive alpha
        Gam(n)=G*j;
        if real(Gam(n))<0, Gam(n)=-Gam(n); end % alpha > 0 always

% A and B parameters
        AA(n)=-x(n)*a-y(n)*b; % for new solution x<0 for ENG
        BB(n)=-y(n)*a+b*x(n);

    end
    close(hwait);
    figure(14)
    clf

    subplot(221)
    loglog(x,y,'xk')
    xlabel('x=t\lambda*\mu_{r_e_a_l}')
    ylabel('y=t\lambda*\mu_{i_m_a_g}')
    title([num2str(SOL),', tan\delta=',num2str(tandel)])

    subplot(222)

```

```

plot(real(zz),imag(zz),'ko')
title([num2str(SOL),' solution, z=z_1+jz_2, z_1=x, z_2=-jy'])
xlabel('real part, z_1 or -x')
ylabel('imaginary part, z_2 or -y')

subplot(223)
plot(real(Gam),imag(Gam),'ko')
title([num2str(SOL),' propagation constant \gamma=\alpha+j\beta'])
xlabel('\alpha, Np/m')
ylabel('\beta, rad/m')

subplot(224)
plot(BB,AA,'k+')
title('A-B classification space')
ylabel('(t/\lambda) A')
xlabel('(t/\lambda) B')
Lmax=floor(max([max(abs(AA)),max(abs(BB))]))+1;
%axis([-Lmax,Lmax,-Lmax,Lmax]),grid
end % end of ENG block

K=[A.' B.' Z.' zz.' Gam.']; % save data for debugging

```

B. MATLAB CODE FOR DPS PERFECT ELECTRIC CONDUCTOR

```
function F=transcend_DPS_PEC_pos(X,a,b)
% a and b are POSITIVE (DPS)
% create complex value from real and imaginary parts
z=X(1,:)+j*X(2,:);

% choose sign of impedance with positive resistance
Z=sqrt(z/(a-j*b));
if real(Z)<0, Z=-Z; end

% choose solution with positive alpha
G=sqrt((a-j*b)*z);
if real(G*j)<0, G=-G; end
f=j*Z*tan(2*pi*G)-1;

% separate real and imaginary parts
F=[real(f); imag(f)];
```

C. MATLAB CODE FOR DNG PERFECT ELECTRIC CONDUCTOR

```
function F=transcend_DNG_PEC_neg(X,a,b)
% a and b are NEGATIVE (DNG)
% create complex value from real and imaginary parts
z=-X(1,:)-j*X(2,:);

% choose sign of impedance with negative resistance
Z=sqrt(z/(-a-j*b));
if real(Z)<0, Z=-Z; end

% choose solution with negative alpha
G=sqrt(z*(-a-j*b)); % explicit Gam not needed
if real(G*j)<0, G=-G; end
f=j*Z*tan(2*pi*G)-1;

% separate real and imaginary parts
F=[real(f); imag(f)];
```

```
function F=transcend_MNG_PEC_neg(X,a,b)
% create complex value from real and imaginary parts
z=-X(1,:)-j*X(2,:);

% choose sign of impedance with negative resistance
Z=sqrt(z/(a-j*b));
if real(Z)<0, Z=-Z; end

% choose solution with negative alpha
G=sqrt(z*(a-j*b)); % explicit Gam not needed
if real(G*j)<0, G=-G; end
f=Z*tanh(j*2*pi*G)-1;

% separate real and imaginary parts
F=[real(f); imag(f)];
```

```
function F=transcend_ENG_PEC_neg(X,a,b)
% create complex value from real and imaginary parts
z=X(1,:)-j*X(2,:);

% choose sign of impedance with positive resistance
Z=sqrt(z/(-a-j*b));
if real(Z)<0, Z=-Z; end

% choose solution with positive alpha
G=sqrt(z*(-a-j*b)); % explicit Gam not needed
if real(G*j)<0, G=-G; end
f=Z*tanh(j*2*pi*G)-1;

% separate real and imaginary parts
F=[real(f); imag(f)];
```

```
% to key in z, a, b check equation solution points
z=9.999999999999998 - 3.000000000000000i;
a=10;
b=3;
G=sqrt(z*(a-j*b))
gam=G*j
sqrt(z/(a-j*b))*j*tan(2*pi*G)-1
```

G. MATLAB CODE TO CHECK ON DPS LOOPS

```
% solve transcendental equation for matched RAM layer over PEC backing
% generate a curve on the universal chart
% also numerator and denominator plots of equation solutions to
% investigate "loops"

clear
clc
digits(64);
tandel=.3;

A=logspace(-2,-0,1000);    % a values for search
B=A*tandel;                % b values for search
N=length(A);
Tol=1e-50;

SOL='DPS';                  % start of search range for each curve
msg=['Computing in progress...'];
hwait=waitbar(0,msg);

%%%%DPS%%%%%%%%DPS%%%%%%%%DPS%%%%%%%%DPS%%%%%%%%DPS%%%%%%%%

xest=[0.5 0.75 1];
xest=[.1 .1 .1];
yest=[.01 .01 .01];
Nest=length(xest);
for i=1:Nest
    for n=1:N
        waitbar((N*(i-1)+n)/N/Nest,hwait);
        a=A(n);
        b=B(n);
        vee(n)=a-j*b;
        x_est=xest(i); y_est=yest(i);
        [z fval]=fsolve(@(X) transcend_DPS_PEC_neg(X,a,b), [x_est; y_est],...
            optimset('TolFun',Tol,'Display','off'));
% save values for check
        x(n)=z(1);
        y(n)=z(2);
        if y(n)<0, y(n)=NaN; end
        zee(n)=x(n)-j*y(n);
        zz(n)=z(1)+j*z(2);
        Z(n)=sqrt(zee(n)/vee(n));
        if real(Z(n))<0, Z(n)=-Z(n); end
        G=sqrt((a-j*b)*zee(n));
```

```

% choose solution with positive alpha
    Gam(n)=G*j;
    if real(Gam(n))<0, Gam(n)=-Gam(n); end % alpha > 0 always
% calculate numerator and denominator
    AA=real(sqrt(zee(n))); BB=imag(sqrt(zee(n)));
    CC=2*pi*sqrt(vee(n));
    Num(n)=tan(CC*AA)+tan(j*CC*BB);
    Den(n)=1-tan(CC*AA)*tan(j*CC*BB);
    Fac(n)=2*pi/CC*(j*AA-BB);
end
Sol=Fac.*Num./Den-1;
figure(1)
if i==1, clf; end
if i==1, s='xk'; end
if i==2, s='xr'; end
if i==3, s='xg'; end
if i==4, s='xb'; end
loglog(x,y,s)
xlabel('x=t/\lambda*\mu_r_e_a_l')
ylabel('y=t/\lambda*\mu_i_m_a_g')
title([num2str(SOL),', tan\delta=',num2str(tandel)])
%axis([1e-4,10,1e-2,10])
hold on
figure(2)
if i==1, clf; end
plot(real(zz),imag(zz),s)
title([num2str(SOL),', solution, z=z_1+jz_2, z_1=x, z_2=-y'])
xlabel('real part, z_1 or x')
ylabel('imaginary part, z_2 or -y')
hold on
figure(3)
if i==1, clf; end
plot(real(Gam),imag(Gam),s)
title([num2str(SOL),', propagation constant \gamma=\alpha+j\beta'])
xlabel('\alpha, Np/m')
ylabel('\beta, rad/m')
hold on
figure(4)
if i==1, clf; end
subplot(221)
plot(real(Num),imag(Num),s)
title([num2str(SOL),', numerator'])
xlabel('real')
ylabel('imag')
hold on

```

```

subplot(222)
plot(real(Den),imag(Den),s)
title([num2str(SOL),' denominator'])
xlabel('real')
ylabel('imag')
hold on
subplot(223)
plot(real(Fac),imag(Fac),s)
title([num2str(SOL),' factor'])
xlabel('real')
ylabel('imag')
hold on
subplot(224)
plot(real(Sol),imag(Sol),s)
title([num2str(SOL),' total'])
xlabel('real')
ylabel('imag')
hold on
figure(5)
if i==1, clf; end
subplot(221)
polar(abs(Num),angle(Num),s)
title([num2str(SOL),' numerator'])
hold on
subplot(222)
polar(abs(Den),angle(Den),s)
title([num2str(SOL),' denominator'])
hold on
subplot(223)
polar(abs(Fac),angle(Fac),s)
title([num2str(SOL),' factor'])
hold on
subplot(224)
polar(abs(Sol),angle(Sol),s)
title([num2str(SOL),' total'])
hold on
end % next start point
close(hwait);
K=[A.' B.' Z.' zz.' Gam.']; % save data for debugging
format long
clc
disp(' a=t/w*Re(epsr)      b=t/w*Re(epsr)      Impedance, Z
      x=t/w*Re(mur)      -y=t/w*Im(mur)      alpha=Re(gam)
      beta=Im(gam)')
disp(K)

```

H. MATLAB CODE FOR UNIVERSAL DESIGN CHART USING SOLVE FUNCTION

```
% use solve for the transcendental equation for DPS
% revised to handle multiple solutions back from solve
clear
clc
format long
Ndgs=10;
disp(['number of digits set at ',num2str(Ndgs)])
digits(Ndgs);
tandel=.5;
A=logspace(-3,1,500);
N=length(A);
B=A*tandel;          % b values for search

%%%%DPS%%%%%%%%DPS%%%%%%%%DPS%%%%%%%%DPS%%%%%%%%DPS%%%%%%%%
figure(1)
clf
for n=1:N
    a=A(n);
    b=B(n);
    disp([num2str(n),' of ',num2str(N),' a=',num2str(a)])
    vee(n)=a-j*b;
    Vee=vee(n);
    if imag(Vee)<0, Vi=['-sqrt(-1)*',num2str(abs(imag(Vee)),Ndgs)]; end
    if imag(Vee)>=0, Vi=['+sqrt(-1)*',num2str(abs(imag(Vee)),Ndgs)]; end
    Sv=[num2str(real(Vee),Ndgs),Vi];
    Eqn=['sqrt(zzz/(',Sv,'))*sqrt(-1)*tan(2*pi*sqrt(',Sv,')*zzz))-1=0'];
    Temp=eval(solve(Eqn,'zzz'));
    solns=size(Temp);
    if solns(1)==1; % one solution returned
        Zee(n)=Temp;
    end
    if solns(1)>1 % two solutions returned
        if imag(Temp(1))<=0, Zee(n)=Temp(1,1); end
        if imag(Temp(2))<=0, Zee(n)=Temp(2,1); end
    end
    X(n)=real(Zee(n)); Y(n)=-imag(Zee(n));
    loglog(X(n),Y(n),'xr')
    hold on
end
xlabel('x=t/\lambda\mu_{r_e_a_l}')
ylabel('y=t/\lambda\mu_{i_m_a_g}')
title(['DPS: tan\delta=',num2str(tandel)])
```


THIS PAGE INTENTIONALLY LEFT BLANK

LIST OF REFERENCES

- [1] Sao Jose dos Campos, "Dielectric Microwave Absorbing Material Processed by Impregnation of Carbon Fiber Fabric with Polyaniline," *Material Research*, vol. 10, no.1, pp. 95-99, 2007.
- [2] H.M. Musal, Jr and D.C. Smith, "Universal Design Chart for Specular Aborbers," *IEEE Transactions on Magnetics*, vol. 26, no. 5, September 1990.
- [3] Andrew A. Houck, Jeffrey B. Brock, Isaac L. Chuang, "Experimental Observations of a left-Handed Material That Obeys Snell's Law," *Physical Review Letters*, vol. 90, no. 13, pp. 137402-1-137404, April 2003.
- [4] Bo-Kai Feng, "Extracting Material Constitutive Parameters from Scattering Parameters," *Master's Thesis*, Naval Postgraduate School, Monterey, California, September 2006.
- [5] Christos Doumenis, "Properties and Applications of Lossy MetaMaterials," *Master's Thesis*, Naval Postgraduate School, Monterey, California, December 2011.
- [6] D.H. Lee and W.S. Park, "A New Material Classification of Lossy Metamaterial," *IEEE Trans. Microwave and Optical Technology Letters*, vol. 53, no. 2, pp. 445-447, February 2011.
- [7] Christopher L. Holloway, Edward F. Kuester, Joshua A. Gordon, John O'Hara, Jim Booth, and David R. Smith, "An Overview of the Theory and Applications of Metasurfaces: The Two-Dimensional Equivalents of Metamaterials," *IEEE Antennas and Propagation Magazine*, vol. 54, no. 2, April 2012.
- [8] Victor Georgievich Veselago, "The Electrodynamics of Substances with Simultaneously Negative Values of ϵ and μ ," *P.N Lebedev Physics Institute*, vol. 10, no. 4, pp. 509-514, Academy of Sciences, USSR, January-February 1968.
- [9] J.B. Pendry, "Negative Refraction Makes a Perfect Lens," *Phys. Rev. Lett.*, vol. 85, pp. 3966, Imperial College, London, 2000.
- [10] J.B. Pendry, A.J. Holden, D.J. Robbins and W.J. Stewart, "Magnetism from conductors and enhanced nonlinear phenomena," *IEEE Trans. on Microwave Theory and techniques*, vol. 47, pp. 2075-2084, 1999.
- [11] D.R. Smith, Willie J. Padilla, D.C. Vier, S.C. Nemat-Nasser, and S. Schultz, "Composite Medium with Simultaneously Negative Permeability and Permittivity," *Physical Review Letters*, vol. 84, no. 18, pp. 4184-4187, May 2000.

- [12] Cihangir Kemal Yuzcelik, “ Radar Absorbing Material Design,” *Master’s Thesis*, Naval Postgraduate School, Monterey, California, September 2003.
- [13] Andrea Alu and Nader Enghetta, “Pairing an Epsilon-Negative Slab With a Mu-Negative Slab: Resonance, Tunneling and Transparency,” *IEEE Trans. on Ant. and Prop.*, Vol. 51, no. 10, pp. 2558-2571, Oct. 2003.
- [14] Andrea Alu and Nader Enghetta, “Peculiar Radar Cross-Section Properties of Double-Negative and Single-Negative Metamaterials,” *Radar Conference 2004 Proceeding of the IEEE*, pp. 91-93, April 2004.

INITIAL DISTRIBUTION LIST

1. Defense Technical Information Center
Ft. Belvoir, Virginia
2. Dudley Knox Library
Naval Postgraduate School
Monterey, California
3. Professor R.Clark Robertson
Chairman, Department of Electrical and Computer Engineering
Naval Postgraduate School
Monterey, California
4. Professor David C. Jenn
Professor, Department of Electrical and Computer Engineering
Naval Postgraduate School
Monterey, California
5. Professor Roberto Cristi
Professor, Department of Electrical and Computer Engineering
Naval Postgraduate School
Monterey, California
6. Professor Tat Soon Yeo
Director, Temasek Defense Systems Institute (TDSI)
National University of Singapore (NUS)
Singapore
7. Ms. Lai Poh Tan
Senior Manager, Temasek Defense Systems Institute (TDSI)
National University of Singapore (NUS)
Singapore
8. Mr. Fong Saik Hay
Chief Technology Officer, Singapore Technologies Engineering (ST Engg)
Singapore
9. Mr. Lee Boon Kwang Vincent
Chief Technology Officer, Singapore Technologies Marine (ST Marine)
Singapore

10. Mr. Ting Choon Boon
Assistant Principal Engineer, Singapore Technologies Marine Ltd (ST Marine)
Singapore